Cell Reports
Medicine

Article

Preclinical development of a chimeric antigen receptor T cell therapy targeting FGFR4 in rhabdomyosarcoma

Graphical abstract

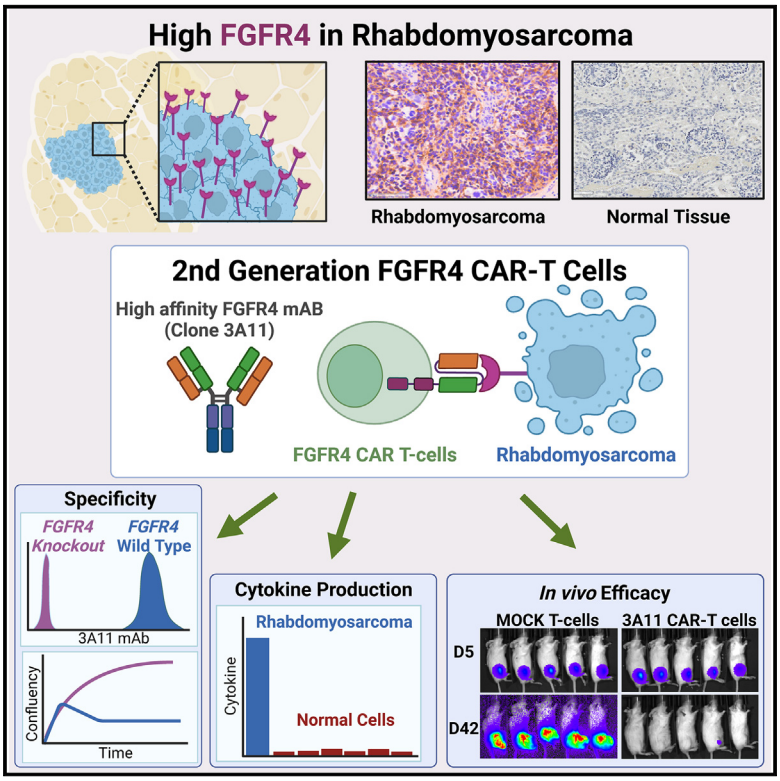

Highlights

- FGFR4 is highly expressed in rhabdomyosarcoma and lowly expressed in healthy human tissue
- FGFR4 is a downstream target of the *PAX3-FOXO1* fusion oncogene
- FGFR4 CAR T cells demonstrate no cytokine release against primary human cells
- FGFR4 CAR T cells eliminate metastatic and intramuscular solid RMS tumors *in vivo*

Authors

Meijie Tian, Jun S. Wei, Nityashree Shivaprasad, ..., Rimas J. Orentas, Adam T. Cheuk, Javed Khan

Correspondence

cheukt@gmail.com (A.T.C.), khanjav@mail.nih.gov (J.K.)

In brief

Tian et al. develop a potent clinical-grade CAR targeting FGFR4 that is highly expressed in rhabdomyosarcoma. FGFR4 CAR T cells show specific cytotoxicity against RMS cell lines and are non-reactive to healthy human primary cells. These CAR T cells eliminate tumors in metastatic and orthotopic mouse models of RMS.

Tian et al., 2023, Cell Reports Medicine *4*, 101212
October 17, 2023
https://doi.org/10.1016/j.xcrm.2023.101212

CellPress

Cell Reports Medicine

CellPress
OPEN ACCESS

Article

Preclinical development of a chimeric antigen receptor T cell therapy targeting FGFR4 in rhabdomyosarcoma

Meijie Tian,[1] Jun S. Wei,[1] Nityashree Shivaprasad,[1] Steven L. Highfill,[2] Berkley E. Gryder,[1] David Milewski,[1] G. Tom Brown,[3] Larry Moses,[2] Hannah Song,[2] Jerry T. Wu,[1] Peter Azorsa,[1] Jeetendra Kumar,[1] Dina Schneider,[4] Hsien-Chao Chou,[1] Young K. Song,[1] Abdelrahman Rahmy,[1] Katherine E. Masih,[1,5] Yong Yean Kim,[1] Brian Belyea,[6] Corinne M. Linardic,[6] Boro Dropulic,[7] Peter M. Sullivan,[8] Poul H. Sorensen,[9] Dimiter S. Dimitrov,[10] John M. Maris,[11] Crystal L. Mackall,[12] Rimas J. Orentas,[8,13] Adam T. Cheuk,[1,14,*] and Javed Khan[1,14,15,*]

[1]Genetics Branch, National Cancer Institute, National Institutes of Health, 37 Convent Drive, Bethesda, MD 20892, USA
[2]Center for Cellular Engineering, Department of Transfusion Medicine, National Institutes of Health Clinical Center, Bethesda, MD 20892, USA
[3]Artificial Intelligence Resource, Center for Cancer Research, National Cancer Institute, NIH, Bethesda, MD 20892, USA
[4]Lentigen Corporation, Miltenyi Bioindustry, 1201 Clopper Road, Gaithersburg, MD 20878, USA
[5]Cancer Research UK Cambridge Institute, University of Cambridge, Cambridge CB2 0RE, UK
[6]Department of Pediatrics, Duke University School of Medicine, Durham, NC 27710, USA
[7]Caring Cross, 708 Quince Orchard Road, Gaithersburg, MD 20878, USA
[8]Ben Towne Center for Childhood Cancer Research, Seattle Children's Research Institute, 1100 Olive Way, Seattle, WA 98101, USA
[9]Department of Molecular Oncology, British Columbia Cancer Research Centre, Vancouver, BC V5Z 1L3, Canada
[10]University of Pittsburgh Department of Medicine, Pittsburgh, PA 15261, USA
[11]Children's Hospital of Philadelphia and Perelman School of Medicine at the University of Pennsylvania, Philadelphia, PA, USA
[12]Department of Pediatrics, Stanford University School of Medicine, Stanford, CA 94305, USA
[13]Department of Pediatrics, University of Washington School of Medicine, Seattle, WA 98101, USA
[14]These authors contributed equally
[15]Lead contact
*Correspondence: cheukt@gmail.com (A.T.C.), khanjav@mail.nih.gov (J.K.)
https://doi.org/10.1016/j.xcrm.2023.101212

SUMMARY

Pediatric patients with relapsed or refractory rhabdomyosarcoma (RMS) have dismal cure rates, and effective therapy is urgently needed. The oncogenic receptor tyrosine kinase fibroblast growth factor receptor 4 (*FGFR4*) is highly expressed in RMS and lowly expressed in healthy tissues. Here, we describe a second-generation FGFR4-targeting chimeric antigen receptor (CAR), based on an anti-human FGFR4-specific murine monoclonal antibody 3A11, as an adoptive T cell treatment for RMS. The 3A11 CAR T cells induced robust cytokine production and cytotoxicity against RMS cell lines *in vitro*. In contrast, a panel of healthy human primary cells failed to activate 3A11 CAR T cells, confirming the selectivity of 3A11 CAR T cells against tumors with high FGFR4 expression. Finally, we demonstrate that 3A11 CAR T cells are persistent *in vivo* and can effectively eliminate RMS tumors in two metastatic and two orthotopic models. Therefore, our study credentials CAR T cell therapy targeting FGFR4 to treat patients with RMS.

INTRODUCTION

Rhabdomyosarcoma (RMS) is the most common soft tissue sarcoma in children, accounting for 5% of all childhood malignancies.[1] Histologically, pediatric RMS is classified into two major subtypes, alveolar RMS (ARMS) and embryonal RMS (ERMS).[1] However, RMS is more accurately defined by the expression of genes related to skeletal muscle differentiation.[1–3] There are two major molecular subtypes of RMS based on the presence or absence of *PAX3/7* gene translocations with *FOXO1*, which are referred to as fusion-positive RMS (FP-RMS) or fusion-negative RMS (FN-RMS), respectively.[2,3] PAX3-FOXO1 is the primary oncogenic driver in FP-RMS, activating a myogenic transcription program,[4] whereas FN-RMSs are primarily driven by mutations in the RAS pathway, including fibroblast growth factor receptor 4 (*FGFR4*).[4–6] Despite clinical trials with multimodal therapies, including surgery, radiation, and aggressive chemotherapy, there has been no significant improvement in clinical outcomes for patients with RMS for over two decades.[7] Because further dose escalation of chemotherapy has shown no benefit, alternative treatment strategies are necessary.

FGFR4 is a cell surface receptor tyrosine kinase that is involved in the regulation of cell proliferation, migration, cell survival, and angiogenesis in RMS.[8,9] FGFR4 expression is lost after differentiation into mature skeletal muscle. And in healthy

skeletal muscle tissue, FGFR4 is only transiently expressed in activated myoblasts in response to injury.[10–13] We previously reported that *FGFR4* is overexpressed in virtually all RMSs, and high expression is associated with poor outcome.[9,10] We also have shown that PAX3-FOXO1 directly targets the *FGFR4* gene locus, where it establishes a super-enhancer, driving its high expression in FP-RMS.[6] Furthermore, approximately 7.5%–10% of FN-RMSs have activating mutations in *FGFR4*.[2,14] Because of these important characteristics in RMS biology, we hypothesized that FGFR4 is an excellent antigen target for immunotherapy for this malignancy.

Chimeric antigen receptor (CAR) T cell therapy targeting cell surface tumor-associated antigens (TAAs) is an attractive treatment modality for tumors with a low mutational burden.[15–17] Since its first report in the 1980s, multiple generations of CAR constructs have been developed. In general, second-generation CAR constructs contain an extracellular domain of single-chain variable fragment (scFv) that binds the target antigen, a CD8α or CD28 hinge and transmembrane domain, and an intracellular domain consisting of a costimulatory receptor (4-1BB and/or CD28) and a CD3ζ domain. When the scFv binds its target antigen, the intracellular costimulatory domain and the CD3ζ domain signal to activate the CAR T cell and induce cytolysis of the target cell.[18] This strategy is rapidly becoming an important treatment option for children with cancer, with dramatic responses in leukemia and lymphoma, resulting in the approval of six CAR T cell therapies targeting CD19 or B cell maturation antigen (BCMA) by the FDA.[19–24] In addition, CAR T cell therapies targeting ganglioside GD2 have recently shown promising clinical responses to neuroblastoma (NB)[25,26] or H3K27M-mutated diffuse midline gliomas.[27] In a phase 1 clinical trial,[28,29] a patient with RMS went into long-term remission after receiving infusions of HER2 CAR T cells, which suggests that RMSs are susceptible to CAR T cell therapy. FGFR4 CAR T cells have been reported to show cytotoxicity against RMS cell lines *in vitro*,[30] and recently, we reported a FGFR4-targeting CAR, which was only effective when combined with anti-myeloid polypharmacy (targeting CSF1R, IDO1, iNOS, transforming growth factor β [TGF-β], PDL1, MIF, and myeloid mis-differentiation).[31] Here, we describe a potent engineered CAR targeting FGFR4 that is currently being developed for a phase 1 clinical trial at the National Cancer Institute (NCI).

RESULTS

FGFR4 is highly expressed in RMS with low or no expression in human healthy tissue including vital organs

We previously reported that *FGFR4* is highly expressed in all RMSs as a diagnostic and prognostic biomarker.[9,10,32] Here, we confirm by RNA sequencing (RNA-seq) that *FGFR4* is highly expressed in both FP-RMS and FN-RMS tumors and cell lines compared with other pediatric solid tumors and healthy human tissues (Figure 1A). To determine if *FGFR4* is also expressed in other adult tumors, we compared its expression in RMS with all tumors of The Cancer Genome Atlas (TCGA). Notably, we found high expression of *FGFR4* in liver hepatocellular carcinoma (LIHC) and cholangiocarcinoma (CHOL), suggesting that FGFR4-targeted therapy may also benefit individuals with these cancers (Figure 1B).

To examine FGFR4 expression at the protein level, we first measured the total FGFR4 level in the RMS cell line RH30 and in healthy tissues using an electrochemiluminescence assay. We found that the RH30 cell line has at least 3-fold higher FGFR4 protein expression (1,348 pg/mg) compared with healthy tissues (2–436 pg/mg) (Figure S1A). To validate these results, we performed western blotting using a commercially available FGFR4-specific monoclonal antibody on RMS and healthy tissues. FGFR4 is expressed in most RMS cell lines, and FP-RMS cell lines consistently expressed higher levels of FGFR4 (Figure S1B). FGFR4 was not detectable in any of the healthy tissues by western analysis (Figure S1C). Next, we performed immunohistochemistry (IHC) to evaluate the expression of FGFR4 protein on tissue microarrays (TMAs) containing both RMS tumors (22 ARMS and 28 ERMS) and healthy tissues (43 different human organs from 1 to 8 different individuals). Strong positive cell membrane staining of FGFR4 was observed in RMS tumors (17/22 [77%] ARMS and 5/28 [18%] ERMS with an H score >100) but not in healthy tissues, including muscle, heart, kidney, liver, and lung (Figures 1C and 1D). Finally, flow cytometry analysis demonstrated high expression of FGFR4 in FP-RMS and in RMS559, an FN-RMS with a FGFR4 driver mutation (V550L)[33] in keeping with western blotting results (Figure 1E). Therefore, our RNA and protein expression data show that FGFR4 is a highly expressed cell surface TAA in RMS cells and primary tumors, while its expression is low or absent in healthy human tissues, demonstrating it is an ideal candidate target for CAR T cell therapy.

FGFR4 is a downstream target of the *PAX3-FOXO1* fusion oncogene

FGFR4 is differentially expressed in RMS, with higher expression in PAX3-FOXO1-driven FP-RMS. Chromatin immunoprecipitation (ChIP) sequencing for the H3K27ac activation mark revealed the presence of super-enhancers in both FP-RMS and FN-RMS tumors and cell lines at the *FGFR4* locus (Figure 2A). Some of these super-enhancers are only seen in myoblasts and myotubes but not in mature skeletal muscle tissues during healthy muscle development (Figure 2A). In addition, we also observed that PAX3-FOXO1 directly binds to these enhancers in FP-RMS cell lines including RH4, RH5, and SCMC (Figure 2A, top). To test whether PAX3-FOXO1 directly upregulates expression of *FGFR4*, we transduced a previously characterized human fibroblast cell line (7250) lacking *FGFR4* expression with a PAX3-FOXO1 lentiviral construct (18). In the PAX3-FOXO1-expressing fibroblasts, we observed that the onco-fusion protein opens up chromatin, recruits BRD4, and establishes super-enhancers, which are indicated by an increase in H3K27ac at the *FGFR4* locus (Figure 2B). These epigenetic changes, as defined by increased chromatin accessibility and deposition of BRD4 and H3K27ac, which are induced by the binding of PAX3-FOXO1, resulted in a dramatically increased *FGFR4* transcription in the fibroblasts (Figure 2B). These results demonstrated that *FGFR4* is a direct downstream target of the fusion protein PAX3-FOXO1 in RMS. In addition, RMS showed the most dependency on FGFR4 among all human cancers in the DepMap (21Q4)

CellPress
OPEN ACCESS

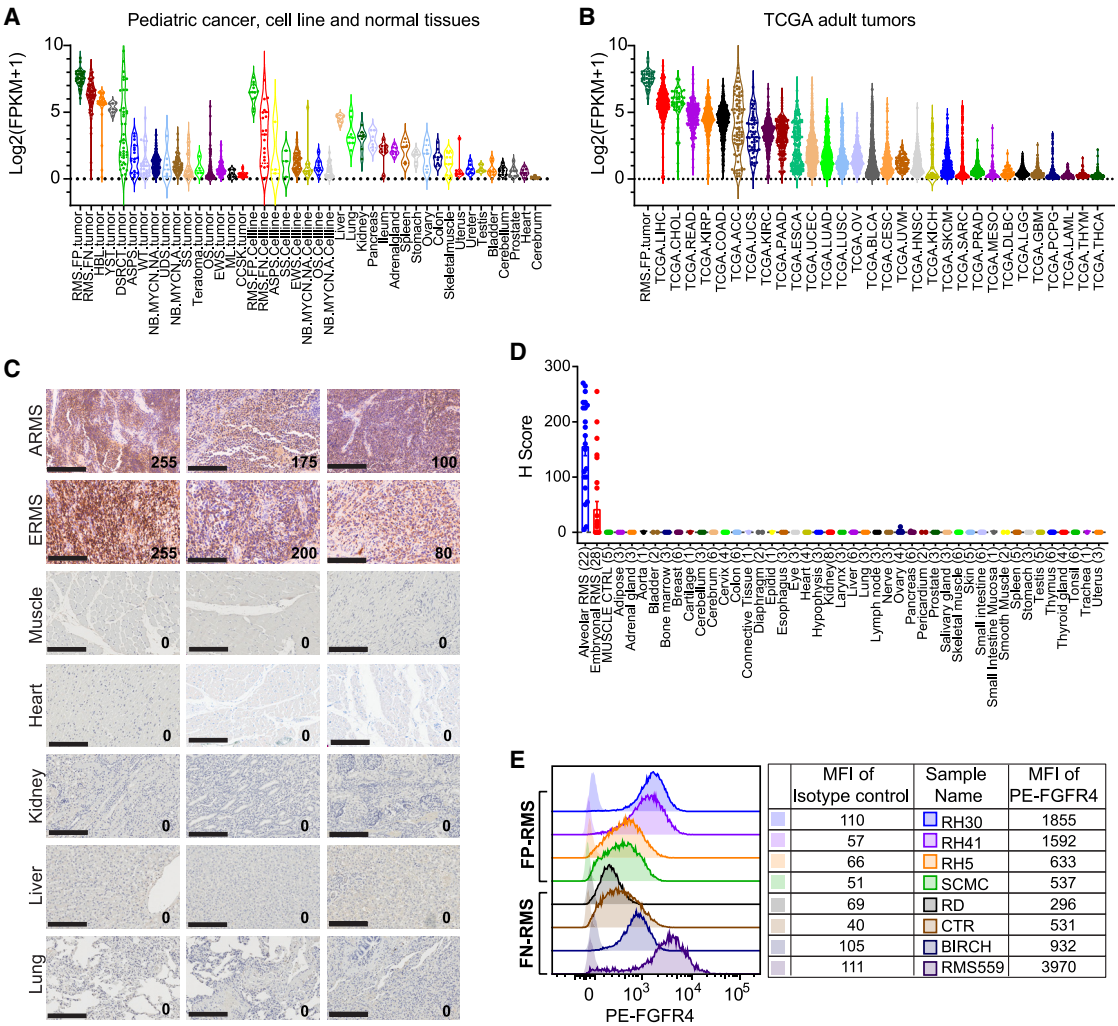

MFI of Isotype control	Sample Name	MFI of PE-FGFR4
110	RH30	1855
57	RH41	1592
66	RH5	633
51	SCMC	537
69	RD	296
40	CTR	531
105	BIRCH	932
111	RMS559	3970

Figure 1. FGFR4 is highly expressed in RMS and other cancers, with low expression in healthy tissue

(A) High expression of *FGFR4* mRNA is found in both FP-RMS and FN-RMS tumors and cell lines compared with other pediatric cancers and healthy tissues. Expression levels measured as FPKM (fragments per kilobase of transcript per million mapped reads) for *FGFR4* are summarized in violin plots with medians and quartiles. ASPS, alveolar soft part sarcoma; CCSK, clear cell sarcoma of the kidney; DSRCT, desmoplastic small round cell tumor; EWS, Ewing sarcoma; HBL, hepatoblastoma; ML, melanoma; NB, neuroblastoma; OS, osteosarcoma; SS, synovial sarcoma; UDS, undifferentiated sarcoma; WT, Wilms tumor; YST, yolk sac tumor).

(B) *FGFR4* mRNA expression in TCGA data shows highest expression in liver hepatocellular carcinoma (LIHC), cholangiocarcinoma (CHOL), and individual tumors of other types. Abbreviations are as per TCGA (https://gdc.cancer.gov/resources-tcga-users/tcga-code-tables/tcga-study-abbreviations).

(C) Representative images of immunohistochemistry (IHC) for FGFR4 show high expression in RMS, with minimum or no expression in healthy organs. H score displayed in bottom right corner, and scale bars, 200 μm.

(D) Summary of membrane-staining H score of FGFR4 IHC of RMS and healthy tissues. Values represent mean ± SEM (error bars).

(E) Representative flow cytometry plots show differential levels of FGFR4 expression on FP-RMS or FN-RMS cell lines. Mean fluorescence intensity (MFI) of FGFR4 on indicated RMS cells is listed in the right table, stained with phycoerythrin (PE)-conjugated anti-human FGFR4 antibody or mouse IgG1 isotype control.

dataset (Figure 2C). Therefore, the *FGFR4* locus, normally transcriptionally active only in developing muscle, becomes activated specifically in RMS.

Development and characterization of the FGFR4-specific antibody 3A11

To develop FGFR4-specific antibodies, we generated hybridoma lines from mice immunized with the human FGFR4 extracellular domain protein. Monoclonal antibody (mAb) 3A11 was the lead clone, demonstrating specific binding to FGFR4$^+$ RMS cell lines RH30 and RMS559 but not to CRISPR FGFR4 knockout RH30 cells (RH30 FGFR4-KO) or the FGFR4$^-$ human fibroblast cell line, 7250 (Figures 3A and 3B). We then constructed a chimeric human mAb 3A11 by fusing the sequence encoding the scFv of 3A11 to the human immunoglobulin G1 (IgG1) Fc domain to generate 3A11 scFvFc antibody and confirmed its specific binding to RMS cell lines only (Figures 3C and 3D). The dissociation constant (K_D) of 3A11 scFvFc was determined

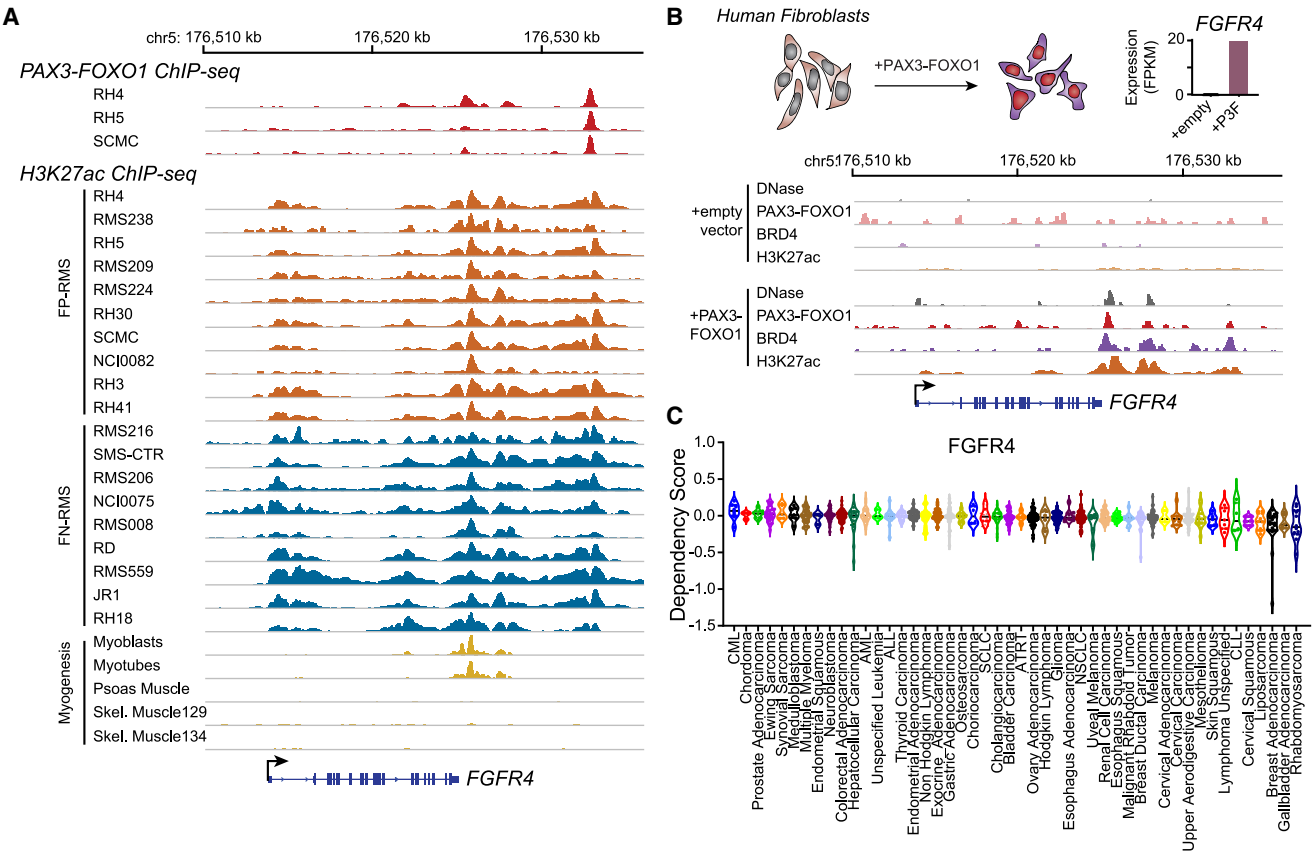

Figure 2. PAX3-FOXO1 establishes a super-enhancer at the *FGFR4* locus, and RMSs are dependent on FGFR4 for survival

(A) PAX3-FOXO1 (top) and H3K27ac (bottom) ChIP-seq at the *FGFR4* locus in FP-RMS cell lines and tumors (orange), FN-RMS cell lines and tumors (blue), and human skeletal muscle cell lines and tissues (gold).

(B) Top: *FGFR4* expression is induced in fibroblasts after introduction of PAX3-FOXO1. Bottom: ChIP-seq demonstrates that PAX3-FOXO1 protein opens chromatin and establishes a super-enhancer at the *FGFR4* locus. Open chromatin was assayed by DNase hypersensitivity; binding of PAX3-FOXO1 and BRD4 as well as chromatin H3K27ac status were assayed by ChIP-seq in human fibroblasts with or without PAX3-FOXO1.

(C) Average dependency score of RMS for FGFR4 was found to be the lowest among all human cancers, suggesting the highest dependency of RMS on this receptor for survival.

to be 4.17 nM using biolayer interferometry (BLI) (Figure 3E). We also confirmed that 3A11 bound only to human FGFR4 but not to other members of the human FGFR family (FGFR1–3) and that it did not show cross-reactivity to mouse FGFR4 by ELISA (Figure 3F). Notably, the 3A11 scFvFc also recognized FGFR4 on RMS cell lines with differing levels of expression (Figure 3G). These data demonstrate that 3A11 scFvFc retains high specificity and affinity for human FGFR4 protein.

3A11 CAR T cells demonstrate specific cytotoxicity *in vitro*

We next aimed to develop a potent clinical-grade FGFR4-targeting CAR by cloning the scFv of 3A11 into a proprietary second-generation CAR vector with a lentiviral backbone (Lentigen Technology) consisting of a 3A11 CAR and a truncated EGFR (tEGFR) safety switch (Figure 4A). The CliniMACS Prodigy system was used to transduce T cells isolated from three healthy donors, and anti-EGFR antibody was used to determine the transduction efficiency, which ranged from 66.5% to 74.7% at day 7 (Figure S2). To assess the *in vitro* efficacy of the 3A11 CAR T cells, we measured their cytotoxicity against RMS cell lines (RH30, RH4, and RMS559), control FGFR4 KO cell lines (RH30 FGFR4-KO and RH4 FGFR4-KO), and the FGFR4^{-} human fibroblast cell line (7250). CAR T cells caused rapid and potent cytotoxicity to RMS cells but not to the FGFR4-KO or the FGFR4^{-} cells at different effector-to-target (E:T) ratios (Figures 4B, 4C, S3A, and S3B). Cytokine production by 3A11 CAR T cells, including interferon γ (IFN-γ), tumor necrosis factor α (TNF-α), and interleukin-2 (IL-2), also increased when the CAR T cells were incubated with FGFR4^{+} cell lines in a dose-dependent manner but not when they were incubated with target-negative cell lines (Figures 4D and S3C). These data demonstrated specific killing activity of 3A11 CAR T cells to FGFR4-expressing target cells.

Clinical-grade 3A11 CAR T cells show no cytotoxicity to primary human cells

Low levels of *FGFR4* mRNA expression are present in some healthy tissues including liver, lung, kidney, and pancreas

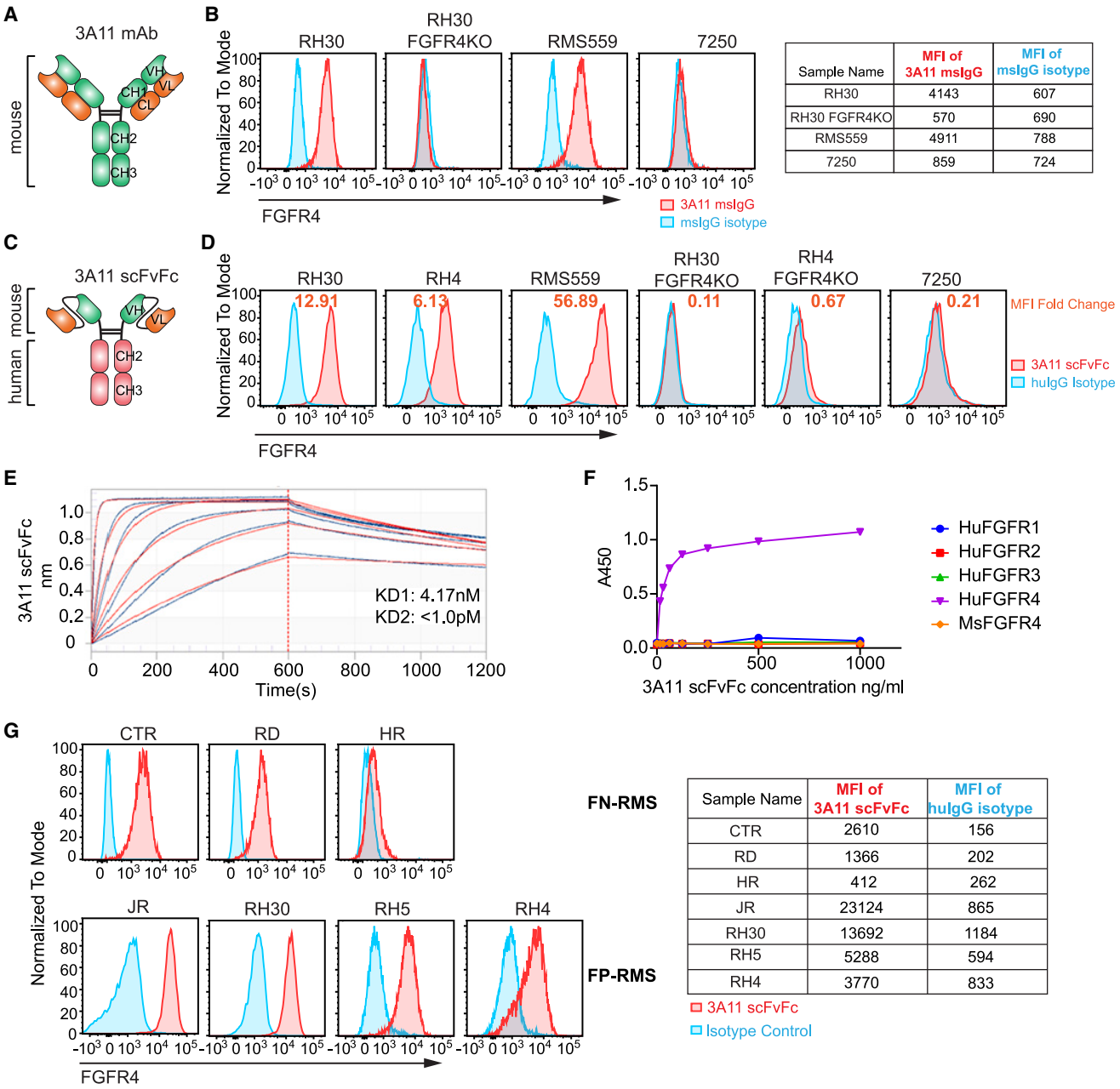

Sample Name	MFI of 3A11 msIgG	MFI of msIgG isotype
RH30	4143	607
RH30 FGFR4KO	570	690
RMS559	4911	788
7250	859	724

Sample Name	MFI of 3A11 scFvFc	MFI of huIgG isotype
CTR	2610	156
RD	1366	202
HR	412	262
JR	23124	865
RH30	13692	1184
RH5	5288	594
RH4	3770	833

Figure 3. Development and characterization of a specific FGFR4 binder from the monoclonal murine antibody 3A11

(A) Structure of the mouse anti-FGFR4 mouse monoclonal antibody (mAb) 3A11.

(B) Representative flow cytometry plots show the specificity of 3A11 mAb by staining with FGFR4^{+} cell lines, FGFR4 KO RH30, or FGFR4^{-} cell 7250. Mouse IgG (msIgG) is used as isotype control for this mouse antibody 3A11.

(C) Structure of anti-FGFR4 antibody 3A11 in scFvFc format fused to the human IgG1 Fc region.

(D) Representative flow cytometry plots show 3A11 scFvFc chimeric antibody specifically binds to FGFR4^{+} cell lines RH30, RH4, and RMS559 but not to the RH30 FGFR4-KO, the RH4 FGFR4-KO, or fibroblast 7250 lines. Human IgG (huIgG) as an isotype control for 3A11 scFvFc. MFI fold change shown as orange font calculated by formula $[MFI(scFvFc) - MFI(huIgG\ isotype)]/MFI(huIgG\ isotype)$.

(E) Binding avidity of FGFR4 scFvFc, using 2-to-1 binding model and global fitting analysis, demonstrates the dissociation constant (K_D) of 3A11 scFvFc against FGFR4 ECD is 4.17 nM.

(F) ELISA shows 3A11 scFvFc only recognizes human FGFR4 but not human FGFR1–3 or mouse FGFR4.

(G) Flow cytometry using 3A11 scFvFc shows FGFR4 is expressed in several RMS cell lines at various levels with higher expression in FP-RMS compared with in FN-RMS. MFI of 3A11 scFvFc or isotype control huIgG staining on above cells is shown in the table on the right.

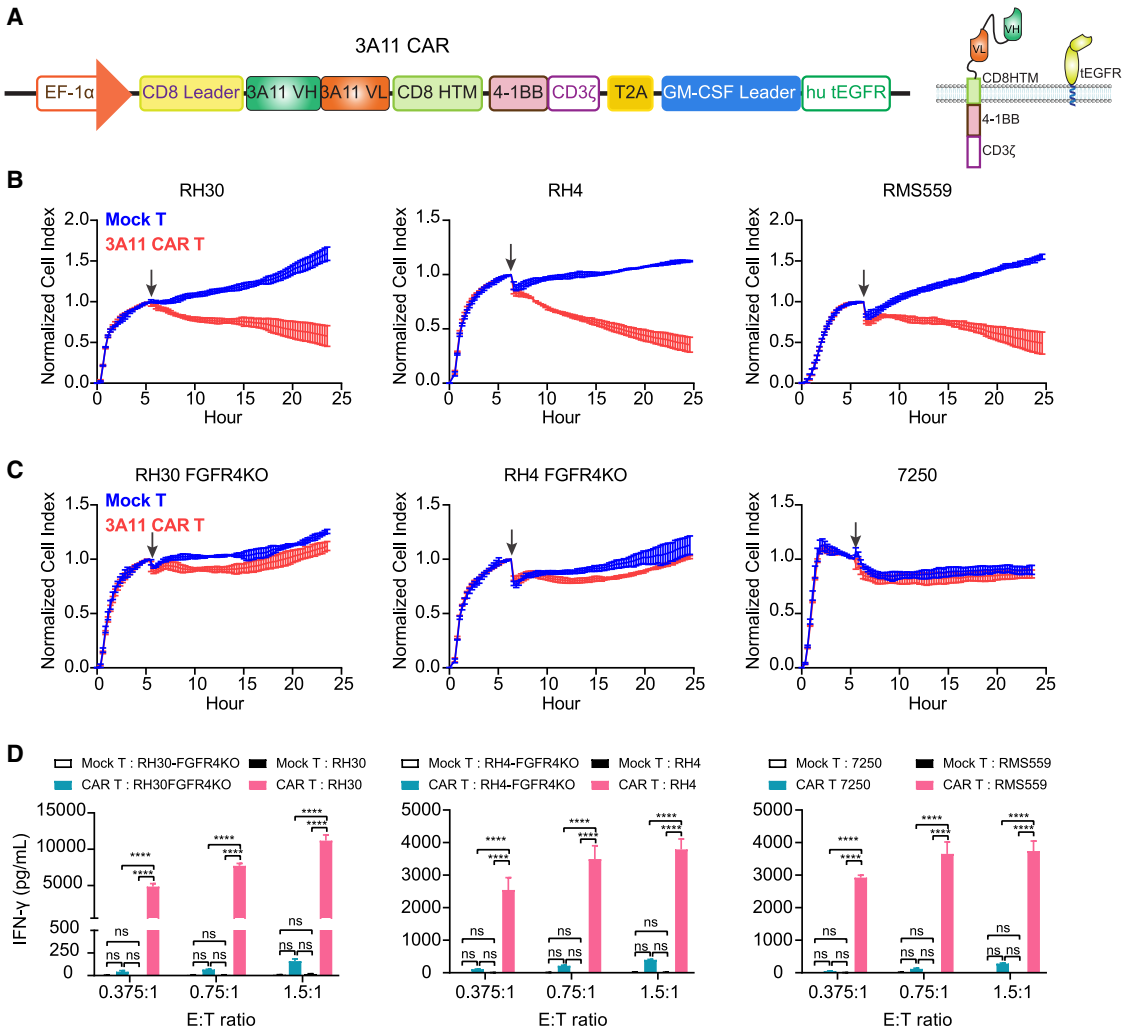

Figure 4. Clinical-grade 3A11 CAR T cells show specific cytotoxicity to FGFR4^{+} cells

(A) Schematic of 3A11 CAR construct targeting FGFR4. HTM, hinge and transmembrane domain; hu tEGFR, human truncated EGFR.

(B) Cytotoxicity assays of 3A11 CAR T cells show potent killing activity toward target RMS cells at an E:T ratio of 0.75:1 in a xCELLigence Real-Time Cell Analysis (RTCA). Vertical black arrows show the time point for adding CAR T cells into a plate seeded with target cells. Representative of n = 3 independent experiments with n = 3 individual donors for (B)–(D). Values represent mean ± SD (standard deviation, error bars).

(C) Cytotoxic assay shows 3A11 CAR does not cause cytolysis to FGFR4-KO or FGFR4^{-} cells at an E:T ratio of 0.75:1. Values represent mean ± SD (error bars).

(D) Cytokine release assay shows 3A11 CAR T cells only release high level of IFN-γ when cocultured with FGFR4-expressing RMS cells (RH30, RH4, or RMS559) rather than the respective FGFR4-KO cell lines or 7250. Values represent mean ± SEM (error bars). Two-way ANOVA is used to compare secreted IFN-γ by mock T or 3A11 CAR T cells cocultured with the target cells by calculating the p value. *p ≤ 0.05; **p ≤ 0.01; ***p ≤ 0.001; ****p ≤ 0.0001; ns: no significant difference.

(Figure 1A). Because CAR T cells require a high density of surface antigen for activation and cytotoxicity,[34,35] we hypothesized that low levels of FGFR4 expression would not initiate CAR T cell reactivity in healthy tissues. To investigate this, we first measured FGFR4 protein expression in multiple primary human cells isolated from healthy organs by flow cytometry using 3A11scFvFc antibody. Slight peak shifts were observed with 3A11 scFvFc against cardiomyocytes, renal epithelial cells including cortical and proximal tubule epithelial cells, HEK293 (embryonic kidney cells), cholangiocytes, and hepatocytes pooled from 10 individuals, suggesting low FGFR4 expression in these healthy cells that is comparable with a FGFR4^{-} control cell line, human fibroblast 7250 (Figure 5A).

To determine the FGFR4 expression threshold for cytotoxicity and cytokine release, we quantified the number of FGFR4 molecules per cell on a panel of RMS cell lines and the healthy embryonal kidney cell line HEK293 and performed coculture studies with the 3A11 CAR T cells. RH30, RH4, and RD with 9,606, 7,447, and 2,341 FGFR4 molecules per cell, respectively, showed significant cytotoxicity and cytokine release (Figure S4), whereas the low expressor cell lines HR (366 FGFR4 molecules per cell) and HEK293 (155) failed to elicit this response (Figures S4C and S4D). Of note, CTR with 3,282 FGFR4 molecules per cell did not induce significant cytotoxicity or cytokine release, indicating that other tumor-intrinsic factors are important to determine sensitivity to CAR T cells (Figures S4C and S4D).

CellPress
OPEN ACCESS

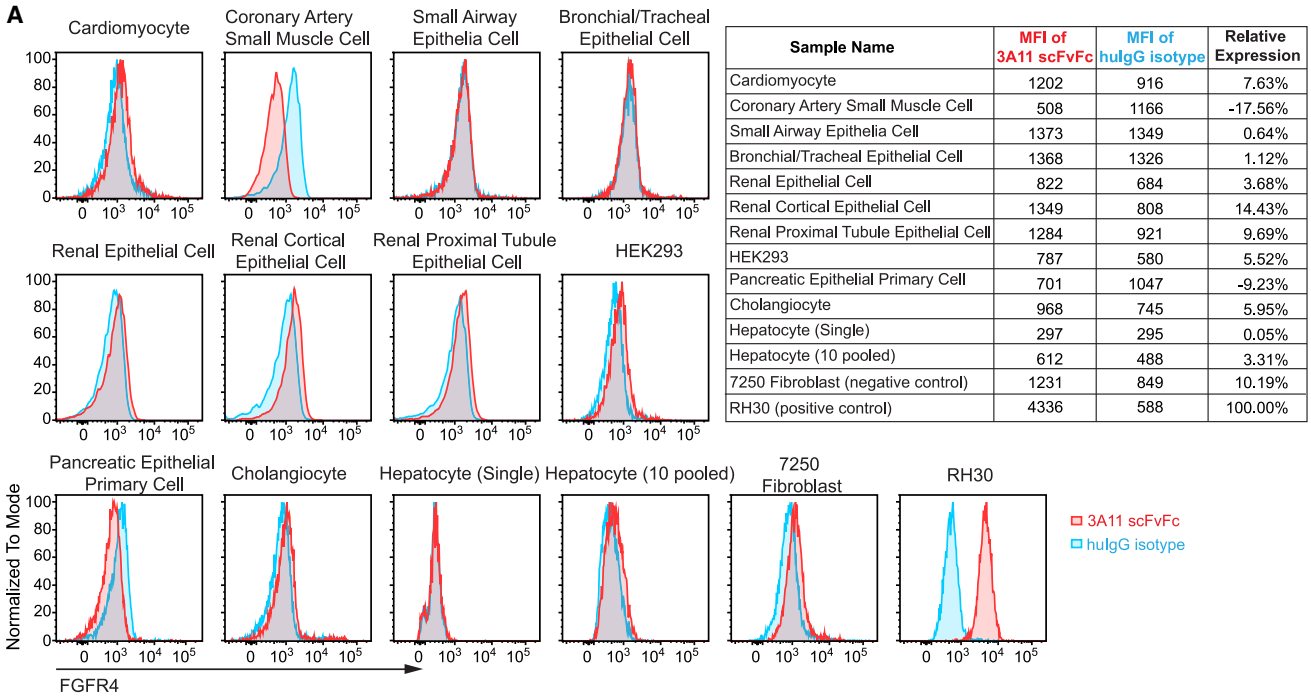

Sample Name	MFI of 3A11 scFvFc	MFI of huIgG isotype	Relative Expression
Cardiomyocyte	1202	916	7.63%
Coronary Artery Small Muscle Cell	508	1166	-17.56%
Small Airway Epithelia Cell	1373	1349	0.64%
Bronchial/Tracheal Epithelial Cell	1368	1326	1.12%
Renal Epithelial Cell	822	684	3.68%
Renal Cortical Epithelial Cell	1349	808	14.43%
Renal Proximal Tubule Epithelial Cell	1284	921	9.69%
HEK293	787	580	5.52%
Pancreatic Epithelial Primary Cell	701	1047	-9.23%
Cholangiocyte	968	745	5.95%
Hepatocyte (Single)	297	295	0.05%
Hepatocyte (10 pooled)	612	488	3.31%
7250 Fibroblast (negative control)	1231	849	10.19%
RH30 (positive control)	4336	588	100.00%

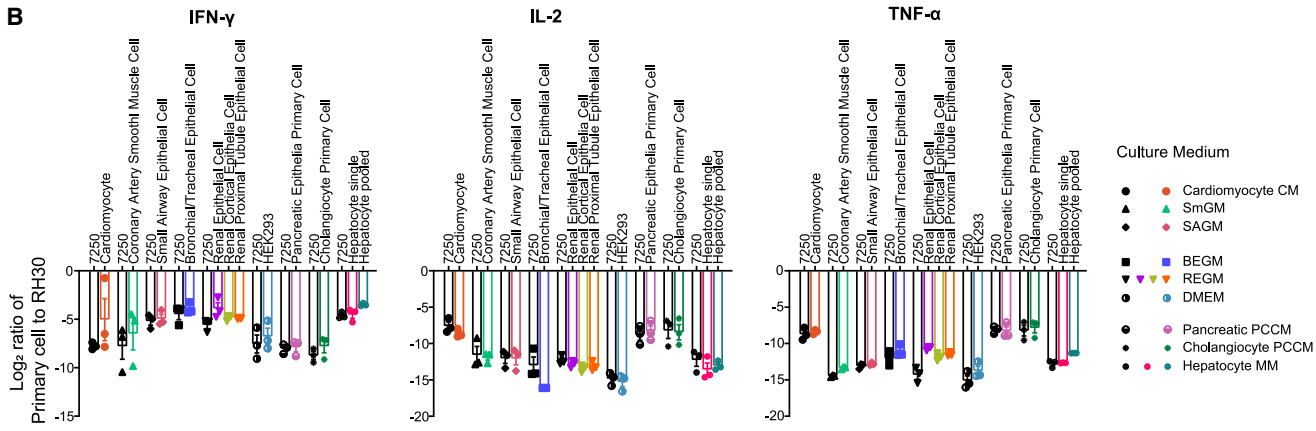

Figure 5. Low or absence of cell surface FGFR4 in primary human cells does not induce cytokine release when cocultured with 3A11 CAR T cells

(A) Representative flow cytometry plots show low or absence of FGFR4 cell surface expression on human cardiomyocytes, renal epithelial cells, renal cortical epithelial cells, renal proximal epithelial cells, HEK293, cholangiocytes, and hepatocytes pooled from 10 individuals using 3A11 scFvFc. MFI of 3A11 scFvFc or huIgG1 isotype control staining on these primary cells is shown in the top right table. Relative FGFR4 expression levels on these primary cells compared with RH30 cells are calculated as *Relative expression* $= \frac{[MFI(scFvFc) - MFI(huIgG\ isotype)]_{Primary\ cell}}{[MFI(scFvFc) - MFI(huIgG\ isotype)]_{RH30}}$.

(B) Log_2 ratio of cytokine (IFN-γ, IL-2, and TNF-α) release in the supernatant, by 3A11 CAR T cells cocultured with primary cells, as indicated, in their respective media, compared with the RMS cell RH30. Cell line 7250 serves as a FGFR4$^-$ control. Values represent n = 3 independent experiments with n = 3 individual donors. Values represent mean ± SEM (error bars).

To further assess the potential for on-target off-tumor reactivity of the 3A11 CAR, we cocultured 3A11 CAR T cells with primary cells and measured cytokine production individually. Again, we did not observe significant production of IFN-γ, IL-2, or TNF-α in coculture experiments using these healthy cells, which was comparable to that of coincubation with 7250 cells lacking FGFR4 expression (Figures 5B and S5). Collectively, these data indicate that 3A11 CAR T cells have little or no on-target off-tumor reactivity to healthy cells expressing low levels of FGFR4.

Clinical-grade 3A11 CAR T cells effectively eliminate metastatic RMS *in vivo*

Next, we evaluated the anti-tumor efficacy of the clinical-grade 3A11 CAR T cells in two *in vivo* metastatic model using both RH30, an FP-RMS cell line, and RMS559, an aggressive

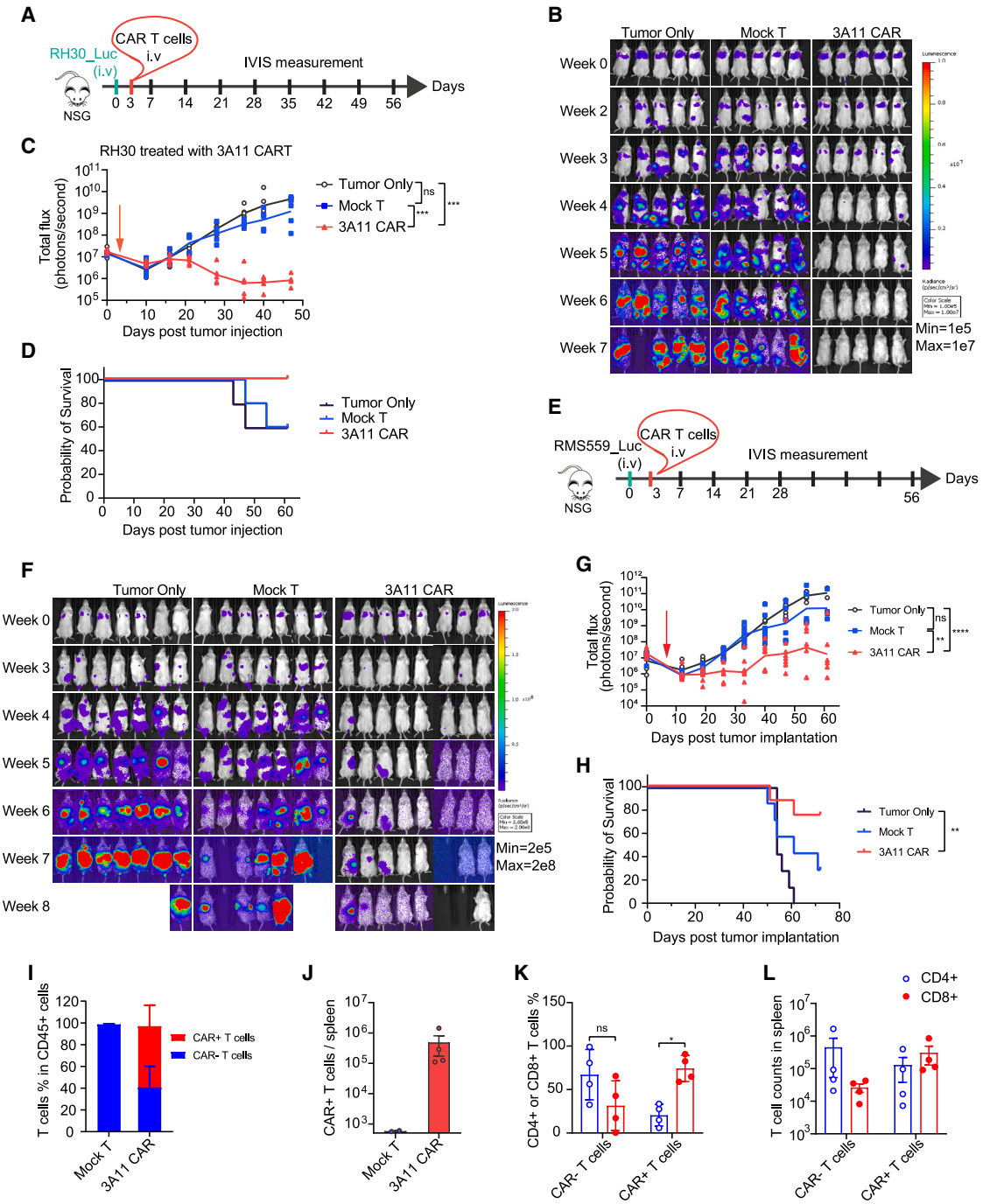

Figure 6. 3A11 CAR T cell shows potent antitumor effect in RH30 and RMS559 metastatic xenograft models

(A) Schematic of an *in vivo* model testing the activity of 3A11 CAR T cells against an RH30 metastatic xenograft model.

(B) Bioluminescent imaging of untreated RH30 xenografts or RH30 xenografts treated with 3E6 mock transduced T cells or 3A11 CAR T cells (n = 5 per group).

(C) Total bioluminescence flux over time of individual mouse treated with HBSS, mock T cells, and 3A11 CAR T cells. Mean (lines) and individual replicates are shown (n = 5 per group). Vertical red arrow indicates the day of T cell infusion, also in (G). Mixed-effects or two-way repeated measures (RM) ANOVA analysis was used to calculate the p value between two groups, respectively. ***$p \leq 0.001$.

(D) Kaplan-Meier survival analysis of mice are shown in (D) (n = 5 per group). Study was ended at day 64 due to the onset of graft-versus-host toxicity (dry skin, weight loss, hunched posture, and fur loss).

(E) Schema of luciferase-expressing RMS559 metastatic model infused with HBSS or 3E6 of mock or CAR T cells on day 3 after tumor inoculation.

(F and G) Bioluminescence images (F) and bioluminescence kinetics (G) of RMS559 cell growth in the metastatic xenograft model. Means and each replicate are shown, n = 7 or 8. Mixed-effects analysis is used to calculate the p values between each two groups individually. **p = 0.0047; ****$p < 0.0001$.

(legend continued on next page)

FN-RMS cell line with a high level of FGFR4 expression (Figure 1E) and a FGFR4 V550L mutation in the intracellular tyrosine kinase domain.[33] First, luciferase-expressing RH30 or RMS559 cells were intravenously injected into NSG mice, and then we treated these mice with 3 million 3A11 CAR T cells, mock T cells, or HBSS vehicle control, 3 days after tumor inoculation, and monitored tumor progression via bioluminescence imaging (Figures 6A and 6E). Mice treated with 3A11 CAR T cells had a significantly lower tumor burden when compared with tumor only ($p = 0.0010$ and $p < 0.0001$ for RH30 and RMS559, respectively) or mock T cells ($p = 0.0001$ and $p = 0.0047$ for RH30 and RMS559, respectively). CAR T cell-treated groups had higher survival probability when compared with HBSS and mock (untransduced) T cell controls (Figures 6B–6D and 6F–6H). The study was ended at day 64 for RH30 and at day 73 for RMS559 due to the onset of graft-versus-host toxicity (dry skin, weight loss, hunched posture, and fur loss). Thus, these data demonstrate that 3A11 CAR T cells effectively suppress and eliminate metastatic RMS tumors *in vivo*.

To characterize T cell persistence, we analyzed the spleens from 3A11 CAR- or mock T cell-treated mice at day 73 post-tumor RMS559 inoculation (day 70 post-CAR or mock T cell infusion). We observed that human CAR^+ T cells were only present in the spleens of 3A11 CAR T cell-treated mice (Figures 6I and 6J), and ~60% of $CD45^+$ cells were CAR^+ T cells (Figure 6I). Interestingly, while CAR T cells were primarily $CD4^+$ before infusion (Figure S2, donor 3), $CD8^+$ CAR T cells were the predominant phenotype at day 70 post-CAR T cell infusion (Figure 6K). This suggests that $CD8^+$ CAR T cells, which participate in the direct killing of the tumor cells,[36] expanded more robustly and persisted in the spleen compared with non-CAR T cell controls (Figure 6L).

3A11 CAR T cells successfully infiltrate into subcutaneous RMS tumor and effectively eradicate intramuscular RMS tumor

Infiltration of CAR T cells into solid tumors is thought to be one of the major barriers of therapeutic efficacy.[37] We evaluated the infiltration ability of 3A11 CAR T cells in a subcutaneous solid RMS RH30 tumor model. RH30 cells were subcutaneously injected into NSG mice, followed by intravenous injection of 3E6 3A11 CAR T cells, mock T cell control, or HBSS vehicle control 3 days after tumor inoculation (Figure S6A). 3A11 CAR T cells significantly inhibited the growth of the RH30 subcutaneous tumor (Figure S6B) and extended the survival of mice compared with mock T cell-treated mice ($p = 0.0002$) (Figure S6C). At day 21 post-tumor injection, four mice from each group were euthanized for immunohistochemistry (IHC). IHC staining showed significant $CD8^+$ and $CD4^+$ T cell infiltration only in the 3A11 CAR T cell-treated tumors but absent in tumors from no treatment or mock T cell control groups (Figures S6D and S6E). These data demonstrate that 3A11 CAR T cells can effectively infiltrate and suppress growth of RMS solid tumors.

To further evaluate the therapeutic efficacy of 3A11 CAR T cells in an orthotopic intramuscular RMS mouse model, luciferase-expressing RH30 cells (9,606 FGFR4 molecules per cell) were injected into the right gastrocnemius muscle of mice. Mock or 3A11 CAR T cells were intravenously infused at day 7 after tumor implantation (Figure 7A). 3A11 CAR T cells significantly controlled the tumor growth compared with the mock T cell-treated group (Figure 7B). Bioluminescence image data also demonstrated that 3A11 CAR T cells rapidly shrank the tumor and eventually eradicated the RMS tumors in 4/5 of mice (Figures 7C and 7D). At the end of this study (day 42 post-tumor implantation), all mock T cell-treated mice were euthanized, due to reaching the endpoint for tumor size, while 3A11 CAR T cell-treated mice were tumor free and survived ($p = 0.0027$; Figure 7E). We then repeated this experiment in another RMS orthotopic model using RMS RH4, which has a moderate FGFR4-expressing level (7,447 molecules per cell) (Figure 7F). Again, 3A11 CAR T cells mediated complete responses in 3/4 RH4-bearing mice (n = 8 per group) and demonstrated significant survival benefit compared with mock T cell-treated mice (Figures 7G–7J). When analyzing circulating blood T cells using flow cytometry, we found that 28%–96% (mean = 72%) $CD45^+$ $CD3^+$ T cells expressed the 3A11 CAR detected by an anti-EGFR antibody in the CAR T cell-treated RH30-bearing mice (Figure 7K), and they retained an average of 7.7E5 circulating CAR^+ T cells per 100 μL in the blood (Figure 7L). Similarly, there is an average of 74% $CD45^+$ $CD3^+$ T cells expressing the 3A11 CAR in CAR T cell-treated RH4-bearing mice (Figures S7A and S7B) and about 4.6E4 CAR^+ T cells per 100 μL circulating in blood at day 42 post-CAR T cell infusion (Figure S7C). Therefore, these data demonstrated the persistence of 3A11 CAR T cells combined with the eradication of RH30 and RH4 orthotopic tumor xenografts for the CAR T cell-treated mice.

DISCUSSION

Current multimodal therapy has improved outcomes of patients with RMS with localized disease. However, for patients with metastatic or relapsed RMS, outcomes remain poor, and dose-escalation chemotherapy has not improved survival.[38–41] RMS tumors, especially FP-RMS, have a low mutation burden, and few tumors have directly actionable driver mutations.[2] Attempts to target mTOR (ClinicalTrials.gov: NCT02567435),[42] HDACs (ClinicalTrials.gov: NCT04299113), the RAS/MAPK pathway,[43,44] and oxidative stress[14] are in various stages of preclinical and clinical testing for RMS. Since RMSs are not intrinsically immunogenic possibly due to their low mutation burden,[2,32] targeting tumor-associated cell surface antigens such as FGFR4 with engineered T cells is an attractive treatment strategy for high-risk RMS. In this study, we report the preclinical

(H) Kaplan-Meier survival analysis of mice bearing RMS559 (7 or 8 mice/group). Log-rank (Mantel-Cox) test is used to compare the survival curves. **p = 0.0028.
(I and J) The frequencies of CAR^+ or CAR^- T cells (I) and total cell counts of CAR^+ T cells (J) in the splenocytes from above mice at 70 days post-mock or CAR T cell infusion are examined by flow cytometry (n = 2 for mock T group, n = 4 for 3A11 CAR T cell-treated group; in mean ± SEM [error bars]).
(K and L) The percentages (K, values represent mean ± SD [error bars]) and total cell counts (L, values represent mean ± SEM [error bars]) of $CD4^+$ and $CD8^+$ cells in CAR^- ($tEGFR^-$) or CAR^+ ($tEGFR^+$) T cells from spleen of 3A11 CAR T cells treated mice are shown. Two-way ANOVA is used to calculate the p values. *p < 0.05.

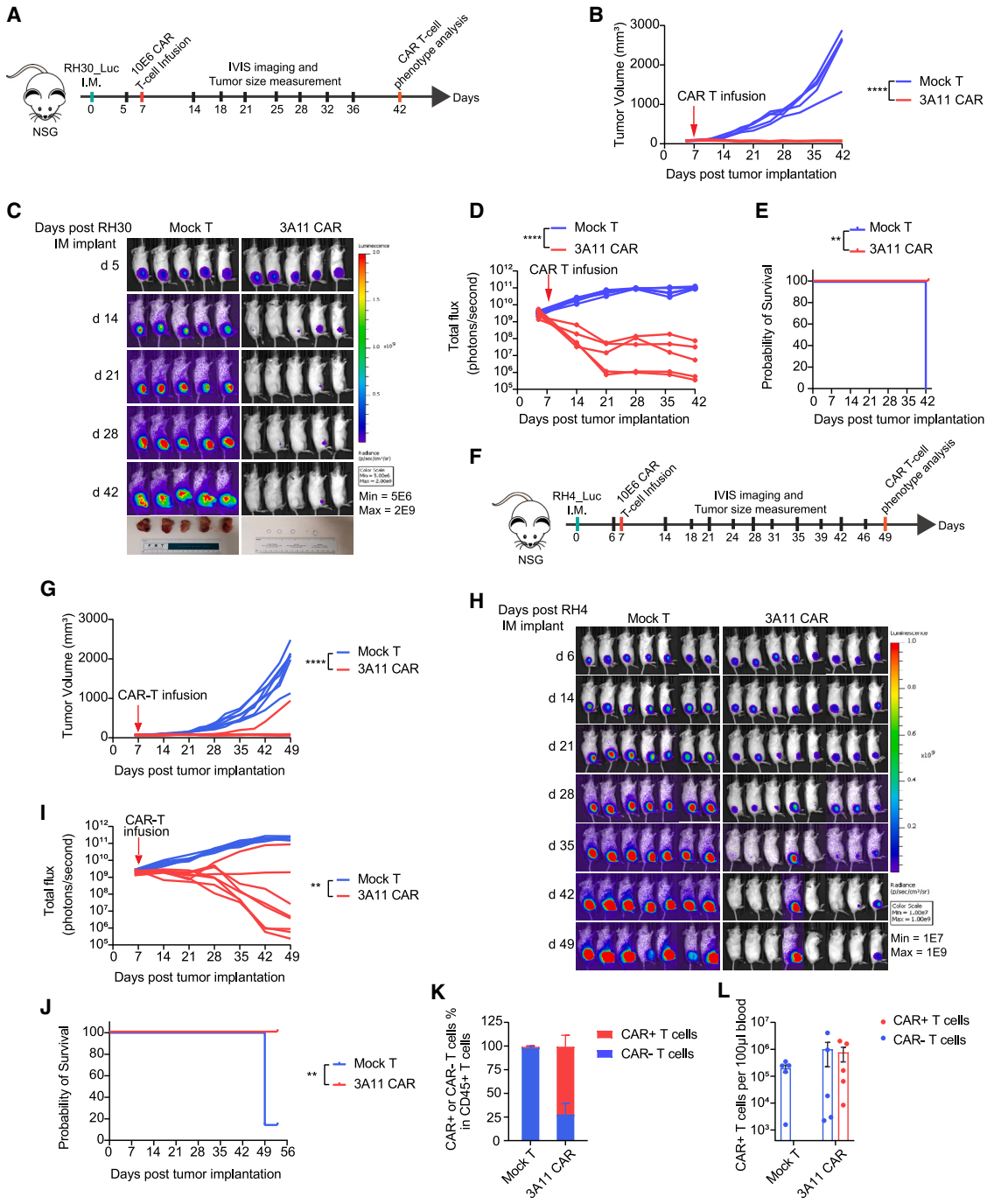

Figure 7. 3A11 CAR T cells effectively eradicated RMS orthotopic intramuscular xenografts in two models

(A) Schema of the RH30 intramuscular xenograft model infused with mock or 10E6 CAR T cells on day 7 post-tumor inoculation.

(B) Tumor size was monitored over 42 days by measurement of leg volume before and after receiving mock or CAR T cell treatment. Vertical red arrow indicates the day of T cell infusion, also in (D), (G), and (I). Each replicate per group is shown, n = 5. Two-way RM ANOVA analysis is used to calculate the p values between two groups. ****$p < 0.0001$.

(C) Bioluminescent images of RH30 intramuscular xenografts growth before and after infusion with mock T cells or 3A11 CAR T cells. The bottom row shows the tumor xenografts dissected from mice legs at the end time point of study.

(D) Total bioluminescence flux (photons per second) over time of individual mouse are shown (n = 5 per group). Two-way RM ANOVA analysis was used to calculate p value between two groups, respectively. ****$p < 0.0001$.

(E) Kaplan-Meier survival analysis of mice bearing orthotopic RH30 tumors. **$p = 0.0027$.

(F) Schema of the RH4 intramuscular xenograft model infused with 10E6 mock or CAR T cells on day 7 post-tumor inoculation.

(legend continued on next page)

development of a CAR T cell therapy targeting FGFR4 in RMS. We identified a high-affinity murine antibody (3A11) that binds FGFR4 without cross-reactivity to other FGF receptor family members or murine FGFR4. 3A11 CAR T cells demonstrated strong FGFR4-specific T cell cytotoxicity to RMS cells *in vitro* and *in vivo* without any significant reactivity to healthy human primary cells.

CAR T cell therapies have shown remarkable response rates against refractory and relapsed leukemia and lymphoma.[37] However, CAR T cell therapy for solid tumors has been less successful, and this is thought to be due to lack of targetable surface antigens, poor infiltration of T cells into the tumor, T cell exhaustion, and various immunosuppressive factors in the tumor microenvironment.[37] Currently, there are several trials and preclinical studies of CAR T cells treating solid tumors, including targeting of PSMA (prostate-specific membrane antigen) for prostate cancers[45]; GD2,[46] ALK,[47] and GPC2[48,49] for NB; mesothelin for lung cancers[50]; HER2 for breast cancer[51] or RMS[28]; EGFRvIII for glioblastoma[52]; and B7-H3 for multiple pediatric and adult solid tumors.[53,54] Our 3A11 CAR T cell therapy showed promising activities against multiple RMS xenograft models, which suggests that relative high levels of FGFR4 expression on the surface of RMS tumor cells and 3A11 CAR design have made CAR T cell therapy effective to treat RMSs. In addition to our study, there has been anecdotal evidence of activity of HER2 CAR T cell therapies in solid tumors, including metastatic RMS.[28,55]

Despite low levels of *FGFR4* mRNA detected in healthy lung, kidney, and liver tissues, we found little or undetectable FGFR4 protein expression in these vital organs by IHC staining and western blotting. However, the Human Protein Atlas (HPA) reports that FGFR4 is expressed at moderate levels in pancreas, kidney, liver, and lung. This discrepancy may be due to the use of a polyclonal FGFR4 antibody by the HPA resulting in non-specific staining. We further confirmed FGFR4 discrepant mRNA and protein expression detection in a wide spectrum of healthy human primary cells by bulk RNA sequencing (data not shown) and flow cytometry. To test if FGFR4 CAR T cells could be activated by human healthy cells, we cocultured CAR T cells with these primary human healthy cells and confirmed that 3A11 CAR T cells do not elicit a cytokine response against these primary cells from vital organs. We also discovered that low FGFR4 density on cells such as HR or HEK293 was unable to trigger cytotoxicity or cytokine release of 3A11 CAR T cells, indicating a safe therapeutic index for FGFR4 CAR T cells. However, we recognize that despite the lack of cytokine release against low-FGFR4-expressing cells in these short-term cultures, it may not preclude toxicity over longer period of observation. Therefore, the ultimate test for FGFR4 CAR T therapy toxicity will be evaluated in our planned human clinical trials. Nevertheless, to mitigate and treat any unforeseen toxicities from the 3A11 CAR T cells, we have engineered a tEGFR tag in our CAR construct that provides a safety switch for rapid depletion of CAR T cells after administration of cetuximab if required.[56]

In conclusion, our study further credentials FGFR4 as an immunotherapy target in RMS, and we have developed a clinical-grade potent CAR specifically targeting human FGFR4. Given the promising preclinical data presented here, 3A11 CAR T cell therapy is currently being developed for a phase 1 clinical trial in patients with RMS at the NCI. In addition, *FGFR4* is also highly expressed in other human cancers including hepatoblastoma, hepatocellular carcinoma, and CHOL. Thus, 3A11 CAR T cell therapy may have a broader applicability to benefit patients with cancers expressing high levels of FGFR4.

Limitations of the study

Our *in vitro* tests showed that 3A11 CAR T cells did not cause cytokine release against either a panel of human primary cells or RMS cells with low FGFR4 expression. However, because our 3A11 binder is specific to human FGFR4 and does not recognize the murine protein, we could not determine the CAR T cells' impact on healthy tissues that may express low levels of FGFR4 in the mouse models we used. Furthermore, the use of immunodeficient mouse models that lack specific immune cells, like regulatory T and myeloid-derived suppressor cells, may have artificially augmented the efficacy of our CAR T cell therapy. Given these factors, the test for toxicity and efficacy will be determined in upcoming human clinical trials.

STAR★METHODS

Detailed methods are provided in the online version of this paper and include the following:

- KEY RESOURCES TABLE
- RESOURCE AVAILABILITY
  - Lead contact
  - Materials availability
  - Data and code availability
- EXPERIMENTAL MODEL AND STUDY PARTICIPANT DETAILS
  - Cell lines
  - Primary cell culture
  - *In vivo* studies
- METHOD DETAILS
  - RNA-seq data analysis
  - Chip-seq data analysis
  - Immunohistochemistry of normal tissue microarray (TMA) and RMS TMA
  - Generation of 3A11 scFvFc

(G) Tumor size was monitored by leg volume. Each replicate per group is shown, n = 7 or 8. Two-way RM ANOVA analysis is used to calculate the p values between two groups. ****$p < 0.0001$.
(H and I) Bioluminescent images of RH4 intramuscular xenografts for individual mice (H) and total bioluminescence flux (I) over time (n = 7 or 8 per group). Mixed-effects analysis was used to calculate p value between two groups, respectively. **$p = 0.0021$.
(J) Kaplan-Meier survival analysis of mice bearing orthotopic RH4 tumors. **$p = 0.0011$.
(K and L) Percentage of CAR^+ and CAR^- in $CD45^+$ $CD3^+$ T cells from peripheral blood mononuclear cells (PBMCs) (K) and total counts of the indicated T cells in 100 μL blood from RH30 orthotopic model (L). Data are shown as each replicate and the mean ± SEM (error bars; n = 5).

- ELISA assay
- 3A11 scFvFc binding affinity determined by octet analysis system
- Electrochemiluminescence assay
- Western blot analysis
- Cell surface protein determination assay
- Generation of the 3A11 CAR construct and lentivirus production
- 3A11 CAR T cell manufacturing
- xCELLigence Real-Time Cell Analysis and cytokine release assay
- *In vitro* toxicity study
- CAR T-cells persistence and exhaustion analysis by flow cytometry
- H&E and immunohistochemistry (IHC) for tumor infiltrating T-cells

- QUANTIFICATION AND STATISTICAL ANALYSIS
  - Statistical analysis

SUPPLEMENTAL INFORMATION

Supplemental information can be found online at https://doi.org/10.1016/j.xcrm.2023.101212.

ACKNOWLEDGMENTS

This work was supported by the Intramural Research Program of NIH, NCI, Center for Cancer Research, which included funds from NIH Cooperative Research and Development Agreement (CRADA, grant no. 3026, titled "Development of Fibroblast Growth Receptor 4 (FGFR4)-targeting Chimeric Antigen Receptors (CARs) for Cancer Therapy"). This research was also supported in part by the Stand Up to Cancer - St. Baldrick's Pediatric Dream Team Translational Research Grant (SU2CAACR-DT1113). Stand Up To Cancer is a division of the Entertainment Industry Foundation. Research grants are administered by the American Association for Cancer Research, the Scientific Partner of SU2C. The authors acknowledge Yanyu Wang of the Lymphokine Testing Section at the NCI Clinical Support Laboratory (CSL) for measuring cytokine production. We acknowledge the NCI Flow Core for providing instruments and services related to flow cytometry. The content of this publication does not necessarily reflect the views or policies of the Department of Health and Human Services, nor does mention of trade names, commercial products, or organizations imply endorsement by the US government.

AUTHOR CONTRIBUTIONS

J. Khan, A.T.C., N.S., and R.J.O. conceived and designed the experiments. A.T.C. and M.T. performed most of the experiments. A.T.C. and M.T. collected, analyzed, and interpreted the data. N.S. performed the antibody characterization studies. S.L.H., L.M., and H.S. manufactured clinical-grade CAR T cells. D.S. and B.D. made the lentiviral-expressing 3A11 CAR. B.E.G., H.-C.C., and Y.K.S. performed ChIP-seq and analyzed the RNA-seq and CRISPR data. G.T.B. manually quantified FGFR4 H score in IHC-stained TMAs. J.T.W. performed western blot assay for examining FGFR4 expression on RMS and healthy tissues. P.A. performed ELISA for 3A11 scFvFc specificity to FGFR1-4. B.B. and C.M.L. from Duke performed FGFR4 IHC staining. D.M., R.J.O., and A.R. provided technical or material support. M.T. organized data and made all figures. A.T.C. and M.T. wrote the original draft. M.T., J.S.W., and J. Khan revised this manuscript. J. Khan., M.T., J.S.W., C.L.M., D.M., A.T.C., K.E.M., Y.Y.K., R.J.O., S.L.H., B.B., C.M.L., D.S., D.S.D., and J. Kumar reviewed and edited the manuscript.

DECLARATION OF INTERESTS

J. Khan, R.J.O., D.S.D., and A.T.C. are inventors on international patent application no. PCT/US2016/052496. The 3A11 CAR sequence is in this patent application (see https://patents.justia.com/patent/11078286) filed on September 19, 2016, titled "Monoclonal antibodies specific for fibroblast growth factor receptor 4 (FGFR4) and methods of their use."

Received: September 22, 2022
Revised: June 12, 2023
Accepted: September 6, 2023
Published: September 28, 2023

REFERENCES

1. Skapek, S.X., Ferrari, A., Gupta, A.A., Lupo, P.J., Butler, E., Shipley, J., Barr, F.G., and Hawkins, D.S. (2019). Rhabdomyosarcoma. Nat. Rev. Dis. Prim. *5*, 1.
2. Shern, J.F., Chen, L., Chmielecki, J., Wei, J.S., Patidar, R., Rosenberg, M., Ambrogio, L., Auclair, D., Wang, J., Song, Y.K., et al. (2014). Comprehensive genomic analysis of rhabdomyosarcoma reveals a landscape of alterations affecting a common genetic axis in fusion-positive and fusion-negative tumors. Cancer Discov. *4*, 216–231.
3. Shern, J.F., Yohe, M.E., and Khan, J. (2015). Pediatric Rhabdomyosarcoma. Crit. Rev. Oncog. *20*, 227–243.
4. Khan, J., Bittner, M.L., Saal, L.H., Teichmann, U., Azorsa, D.O., Gooden, G.C., Pavan, W.J., Trent, J.M., and Meltzer, P.S. (1999). cDNA microarrays detect activation of a myogenic transcription program by the PAX3-FKHR fusion oncogene. Proc. Natl. Acad. Sci. USA *96*, 13264–13269.
5. Gryder, B.E., Wachtel, M., Chang, K., El Demerdash, O., Aboreden, N.G., Mohammed, W., Ewert, W., Pomella, S., Rota, R., Wei, J.S., et al. (2020). Miswired Enhancer Logic Drives a Cancer of the Muscle Lineage. iScience *23*, 101103.
6. Gryder, B.E., Yohe, M.E., Chou, H.C., Zhang, X., Marques, J., Wachtel, M., Schaefer, B., Sen, N., Song, Y., Gualtieri, A., et al. (2017). PAX3-FOXO1 Establishes Myogenic Super Enhancers and Confers BET Bromodomain Vulnerability. Cancer Discov. *7*, 884–899.
7. Weigel, B.J., Lyden, E., Anderson, J.R., Meyer, W.H., Parham, D.M., Rodeberg, D.A., Michalski, J.M., Hawkins, D.S., and Arndt, C.A.S. (2016). Intensive Multiagent Therapy, Including Dose-Compressed Cycles of Ifosfamide/Etoposide and Vincristine/Doxorubicin/Cyclophosphamide, Irinotecan, and Radiation, in Patients With High-Risk Rhabdomyosarcoma: A Report From the Children's Oncology Group. J. Clin. Oncol. *34*, 117–122.
8. Crose, L.E.S., Etheridge, K.T., Chen, C., Belyea, B., Talbot, L.J., Bentley, R.C., and Linardic, C.M. (2012). FGFR4 blockade exerts distinct antitumorigenic effects in human embryonal versus alveolar rhabdomyosarcoma. Clin. Cancer Res. *18*, 3780–3790.
9. Taylor, J.G., Cheuk, A.T., Tsang, P.S., Chung, J.Y., Song, Y.K., Desai, K., Yu, Y., Chen, Q.R., Shah, K., Youngblood, V., et al. (2009). Identification of FGFR4-activating mutations in human rhabdomyosarcomas that promote metastasis in xenotransplanted models. J. Clin. Invest. *119*, 3395–3407.
10. Khan, J., Wei, J.S., Ringnér, M., Saal, L.H., Ladanyi, M., Westermann, F., Berthold, F., Schwab, M., Antonescu, C.R., Peterson, C., and Meltzer, P.S. (2001). Classification and diagnostic prediction of cancers using gene expression profiling and artificial neural networks. Nat. Med. *7*, 673–679.
11. Zhao, P., and Hoffman, E.P. (2004). Embryonic myogenesis pathways in muscle regeneration. Dev. Dynam. *229*, 380–392.
12. Lagha, M., Kormish, J.D., Rocancourt, D., Manceau, M., Epstein, J.A., Zaret, K.S., Relaix, F., and Buckingham, M.E. (2008). Pax3 regulation of FGF signaling affects the progression of embryonic progenitor cells into the myogenic program. Genes Dev. *22*, 1828–1837.
13. Zhao, P., Caretti, G., Mitchell, S., McKeehan, W.L., Boskey, A.L., Pachman, L.M., Sartorelli, V., and Hoffman, E.P. (2006). Fgfr4 is required for

effective muscle regeneration in vivo. Delineation of a MyoD-Tead2-Fgfr4 transcriptional pathway. J. Biol. Chem. *281*, 429–438.

14. Chen, X., Stewart, E., Shelat, A.A., Qu, C., Bahrami, A., Hatley, M., Wu, G., Bradley, C., McEvoy, J., Pappo, A., et al. (2013). Targeting oxidative stress in embryonal rhabdomyosarcoma. Cancer Cell *24*, 710–724.
15. Lee, D.W., Kochenderfer, J.N., Stetler-Stevenson, M., Cui, Y.K., Delbrook, C., Feldman, S.A., Fry, T.J., Orentas, R., Sabatino, M., Shah, N.N., et al. (2015). T cells expressing CD19 chimeric antigen receptors for acute lymphoblastic leukaemia in children and young adults: a phase 1 dose-escalation trial. Lancet *385*, 517–528.
16. Grupp, S.A., Kalos, M., Barrett, D., Aplenc, R., Porter, D.L., Rheingold, S.R., Teachey, D.T., Chew, A., Hauck, B., Wright, J.F., et al. (2013). Chimeric antigen receptor-modified T cells for acute lymphoid leukemia. N. Engl. J. Med. *368*, 1509–1518.
17. Majzner, R.G., Heitzeneder, S., and Mackall, C.L. (2017). Harnessing the Immunotherapy Revolution for the Treatment of Childhood Cancers. Cancer Cell *31*, 476–485.
18. Sadelain, M., Brentjens, R., and Rivière, I. (2013). The basic principles of chimeric antigen receptor design. Cancer Discov. *3*, 388–398.
19. Bouchkouj, N., Kasamon, Y.L., de Claro, R.A., George, B., Lin, X., Lee, S., Blumenthal, G.M., Bryan, W., McKee, A.E., and Pazdur, R. (2019). FDA Approval Summary: Axicabtagene Ciloleucel for Relapsed or Refractory Large B-cell Lymphoma. Clin. Cancer Res. *25*, 1702–1708.
20. Bouchkouj, N., Zimmerman, M., Kasamon, Y.L., Wang, C., Dai, T., Xu, Z., Wang, X., Theoret, M., Purohit-Sheth, T., and George, B. (2022). FDA Approval Summary: Axicabtagene Ciloleucel for Relapsed or Refractory Follicular Lymphoma. Oncol.
21. Haso, W., Lee, D.W., Shah, N.N., Stetler-Stevenson, M., Yuan, C.M., Pastan, I.H., Dimitrov, D.S., Morgan, R.A., FitzGerald, D.J., Barrett, D.M., et al. (2013). Anti-CD22-chimeric antigen receptors targeting B-cell precursor acute lymphoblastic leukemia. Blood *121*, 1165–1174.
22. Kasamon, Y.L., Price, L.S.L., Okusanya, O.O., Richardson, N.C., Li, R.J., Ma, L., Wu, Y.T., Theoret, M., Pazdur, R., and Gormley, N.J. (2021). FDA Approval Summary: Selinexor for Relapsed or Refractory Diffuse Large B-Cell Lymphoma. Oncol. *26*, 879–886.
23. O'Leary, M.C., Lu, X., Huang, Y., Lin, X., Mahmood, I., Przepiorka, D., Gavin, D., Lee, S., Liu, K., George, B., et al. (2019). FDA Approval Summary: Tisagenlecleucel for Treatment of Patients with Relapsed or Refractory B-cell Precursor Acute Lymphoblastic Leukemia. Clin. Cancer Res. *25*, 1142–1146.
24. Sharma, P., Kanapuru, B., George, B., Lin, X., Xu, Z., Bryan, W.W., Pazdur, R., and Theoret, M.R. (2022). FDA Approval Summary: Idecabtagene Vicleucel for Relapsed or Refractory Multiple Myeloma. Clin. Cancer Res. *28*, 1759–1764.
25. Heczey, A., Louis, C.U., Savoldo, B., Dakhova, O., Durett, A., Grilley, B., Liu, H., Wu, M.F., Mei, Z., Gee, A., et al. (2017). CAR T Cells Administered in Combination with Lymphodepletion and PD-1 Inhibition to Patients with Neuroblastoma. Mol. Ther. *25*, 2214–2224.
26. Straathof, K., Flutter, B., Wallace, R., Jain, N., Loka, T., Depani, S., Wright, G., Thomas, S., Cheung, G.W.K., Gileadi, T., et al. (2020). Antitumor activity without on-target off-tumor toxicity of GD2-chimeric antigen receptor T cells in patients with neuroblastoma. Sci. Transl. Med. *12*, eabd6169.
27. Majzner, R.G., Ramakrishna, S., Yeom, K.W., Patel, S., Chinnasamy, H., Schultz, L.M., Richards, R.M., Jiang, L., Barsan, V., Mancusi, R., et al. (2022). GD2-CAR T cell therapy for H3K27M-mutated diffuse midline gliomas. Nature *603*, 934–941.
28. Hegde, M., Joseph, S.K., Pashankar, F., DeRenzo, C., Sanber, K., Navai, S., Byrd, T.T., Hicks, J., Xu, M.L., Gerken, C., et al. (2020). Tumor response and endogenous immune reactivity after administration of HER2 CAR T cells in a child with metastatic rhabdomyosarcoma. Nat. Commun. *11*, 3549.
29. Mitra, S., Sydow, S., Magnusson, L., Piccinelli, P., Törnudd, L., Øra, I., Ljungman, G., Sandgren, J., Gisselsson, D., and Mertens, F. (2022). Amplification of ERBB2 (HER2) in embryonal rhabdomyosarcoma: A potential treatment target in rare cases? Genes Chromosomes Cancer *61*, 5–9.
30. Alijaj, N., Moutel, S., Gouveia, Z.L., Gray, M., Roveri, M., Dzhumashev, D., Weber, F., Meier, G., Luciani, P., Rössler, J.K., et al. (2020). Novel FGFR4-Targeting Single-Domain Antibodies for Multiple Targeted Therapies against Rhabdomyosarcoma. Cancers *12*, 3313.
31. Sullivan, P.M., Kumar, R., Li, W., Hoglund, V., Wang, L., Zhang, Y., Shi, M., Beak, D., Cheuk, A., Jensen, M.C., et al. (2022). FGFR4-targeted chimeric antigen receptors (CARs) combined with anti-myeloid poly-pharmacy effectively treats orthotopic rhabdomyosarcoma. Mol. Cancer Therapeut. *21*, 1608–1621.
32. Brohl, A.S., Sindiri, S., Wei, J.S., Milewski, D., Chou, H.C., Song, Y.K., Wen, X., Kumar, J., Reardon, H.V., Mudunuri, U.S., et al. (2021). Immuno-transcriptomic profiling of extracranial pediatric solid malignancies. Cell Rep. *37*, 110047.
33. Shukla, N., Ameur, N., Yilmaz, I., Nafa, K., Lau, C.Y., Marchetti, A., Borsu, L., Barr, F.G., and Ladanyi, M. (2012). Oncogene mutation profiling of pediatric solid tumors reveals significant subsets of embryonal rhabdomyosarcoma and neuroblastoma with mutated genes in growth signaling pathways. Clin. Cancer Res. *18*, 748–757.
34. Heitzeneder, S., Bosse, K.R., Zhu, Z., Zhelev, D., Majzner, R.G., Radosevich, M.T., Dhingra, S., Sotillo, E., Buongervino, S., Pascual-Pasto, G., et al. (2022). GPC2-CAR T cells tuned for low antigen density mediate potent activity against neuroblastoma without toxicity. Cancer Cell *40*, 53–69.e9.
35. Majzner, R.G., Rietberg, S.P., Sotillo, E., Dong, R., Vachharajani, V.T., Labanieh, L., Myklebust, J.H., Kadapakkam, M., Weber, E.W., Tousley, A.M., et al. (2020). Tuning the Antigen Density Requirement for CAR T-cell Activity. Cancer Discov. *10*, 702–723.
36. Boulch, M., Cazaux, M., Loe-Mie, Y., Thibaut, R., Corre, B., Lemaître, F., Grandjean, C.L., Garcia, Z., and Bousso, P. (2021). A cross-talk between CAR T cell subsets and the tumor microenvironment is essential for sustained cytotoxic activity. Sci. Immunol. *6*, eabd4344.
37. June, C.H., O'Connor, R.S., Kawalekar, O.U., Ghassemi, S., and Milone, M.C. (2018). CAR T cell immunotherapy for human cancer. Science *359*, 1361–1365.
38. Bisogno, G., Ferrari, A., Prete, A., Messina, C., Basso, E., Cecchetto, G., Indolfi, P., Scarzello, G., D'Angelo, P., De Sio, L., et al. (2009). Sequential high-dose chemotherapy for children with metastatic rhabdomyosarcoma. Eur. J. Cancer *45*, 3035–3041.
39. Oberlin, O., Rey, A., Lyden, E., Bisogno, G., Stevens, M.C.G., Meyer, W.H., Carli, M., and Anderson, J.R. (2008). Prognostic factors in metastatic rhabdomyosarcomas: results of a pooled analysis from United States and European cooperative groups. J. Clin. Oncol. *26*, 2384–2389.
40. Weigel, B.J., Breitfeld, P.P., Hawkins, D., Crist, W.M., and Baker, K.S. (2001). Role of high-dose chemotherapy with hematopoietic stem cell rescue in the treatment of metastatic or recurrent rhabdomyosarcoma. J. Pediatr. Hematol. Oncol. *23*, 272–276.
41. Walterhouse, D.O., Hoover, M.L., Marymont, M.A., and Kletzel, M. (1999). High-dose chemotherapy followed by peripheral blood stem cell rescue for metastatic rhabdomyosarcoma: the experience at Chicago Children's Memorial Hospital. Med. Pediatr. Oncol. *32*, 88–92.
42. Mascarenhas, L., Chi, Y.Y., Hingorani, P., Anderson, J.R., Lyden, E.R., Rodeberg, D.A., Indelicato, D.J., Kao, S.C., Dasgupta, R., Spunt, S.L., et al. (2019). Randomized Phase II Trial of Bevacizumab or Temsirolimus in Combination With Chemotherapy for First Relapse Rhabdomyosarcoma: A Report From the Children's Oncology Group. J. Clin. Oncol. *37*, 2866–2874.
43. Yohe, M.E., Gryder, B.E., Shern, J.F., Song, Y.K., Chou, H.C., Sindiri, S., Mendoza, A., Patidar, R., Zhang, X., Guha, R., et al. (2018). MEK inhibition induces MYOG and remodels super-enhancers in RAS-driven rhabdomyosarcoma. Sci. Transl. Med. *10*, eaan4470.

44. Odeniyide, P., Yohe, M.E., Pollard, K., Vaseva, A.V., Calizo, A., Zhang, L., Rodriguez, F.J., Gross, J.M., Allen, A.N., Wan, X., et al. (2022). Correction: Targeting farnesylation as a novel therapeutic approach in HRAS-mutant rhabdomyosarcoma. Oncogene *41*, 3037.

45. Santoro, S.P., Kim, S., Motz, G.T., Alatzoglou, D., Li, C., Irving, M., Powell, D.J., Jr., and Coukos, G. (2015). T cells bearing a chimeric antigen receptor against prostate-specific membrane antigen mediate vascular disruption and result in tumor regression. Cancer Immunol. Res. *3*, 68–84.

46. Louis, C.U., Savoldo, B., Dotti, G., Pule, M., Yvon, E., Myers, G.D., Rossig, C., Russell, H.V., Diouf, O., Liu, E., et al. (2011). Antitumor activity and long-term fate of chimeric antigen receptor-positive T cells in patients with neuroblastoma. Blood *118*, 6050–6056.

47. Walker, A.J., Majzner, R.G., Zhang, L., Wanhainen, K., Long, A.H., Nguyen, S.M., Lopomo, P., Vigny, M., Fry, T.J., Orentas, R.J., and Mackall, C.L. (2017). Tumor Antigen and Receptor Densities Regulate Efficacy of a Chimeric Antigen Receptor Targeting Anaplastic Lymphoma Kinase. Mol. Ther. *25*, 2189–2201.

48. Bosse, K.R., Raman, P., Zhu, Z., Lane, M., Martinez, D., Heitzeneder, S., Rathi, K.S., Kendsersky, N.M., Randall, M., Donovan, L., et al. (2017). Identification of GPC2 as an Oncoprotein and Candidate Immunotherapeutic Target in High-Risk Neuroblastoma. Cancer Cell *32*, 295–309.e12.

49. Li, N., Fu, H., Hewitt, S.M., Dimitrov, D.S., and Ho, M. (2017). Therapeutically targeting glypican-2 via single-domain antibody-based chimeric antigen receptors and immunotoxins in neuroblastoma. Proc. Natl. Acad. Sci. USA *114*, E6623–E6631.

50. Morello, A., Sadelain, M., and Adusumilli, P.S. (2016). Mesothelin-Targeted CARs: Driving T Cells to Solid Tumors. Cancer Discov. *6*, 133–146.

51. Sun, M., Shi, H., Liu, C., Liu, J., Liu, X., and Sun, Y. (2014). Construction and evaluation of a novel humanized HER2-specific chimeric receptor. Breast Cancer Res. *16*, R61.

52. Johnson, L.A., Scholler, J., Ohkuri, T., Kosaka, A., Patel, P.R., McGettigan, S.E., Nace, A.K., Dentchev, T., Thekkat, P., Loew, A., et al. (2015). Rational development and characterization of humanized anti-EGFR variant III chimeric antigen receptor T cells for glioblastoma. Sci. Transl. Med. *7*, 275ra22.

53. Du, H., Hirabayashi, K., Ahn, S., Kren, N.P., Montgomery, S.A., Wang, X., Tiruthani, K., Mirlekar, B., Michaud, D., Greene, K., et al. (2019). Antitumor Responses in the Absence of Toxicity in Solid Tumors by Targeting B7-H3 via Chimeric Antigen Receptor T Cells. Cancer Cell *35*, 221–237.e8.

54. Majzner, R.G., Theruvath, J.L., Nellan, A., Heitzeneder, S., Cui, Y., Mount, C.W., Rietberg, S.P., Linde, M.H., Xu, P., Rota, C., et al. (2019). CAR T Cells Targeting B7-H3, a Pan-Cancer Antigen, Demonstrate Potent Preclinical Activity Against Pediatric Solid Tumors and Brain Tumors. Clin. Cancer Res. *25*, 2560–2574.

55. Navai, S.A., Derenzo, C., Joseph, S., Sanber, K., Byrd, T., Zhang, H., Mata, M., Gerken, C., Shree, A., Mathew, P.R., et al. (2019). Administration of HER2-CAR T cells after lymphodepletion safely improves T cell expansion and induces clinical responses in patients with advanced sarcomas. In Proceedings of the 110th Annual Meeting of the American Association for Cancer Research. Abstract nr LB-147/4.

56. Paszkiewicz, P.J., Fräßle, S.P., Srivastava, S., Sommermeyer, D., Hudecek, M., Drexler, I., Sadelain, M., Liu, L., Jensen, M.C., Riddell, S.R., and Busch, D.H. (2016). Targeted antibody-mediated depletion of murine CD19 CAR T cells permanently reverses B cell aplasia. J. Clin. Invest. *126*, 4262–4272.

57. Chang, W., Brohl, A.S., Patidar, R., Sindiri, S., Shern, J.F., Wei, J.S., Song, Y.K., Yohe, M.E., Gryder, B., Zhang, S., et al. (2016). MultiDimensional ClinOmics for Precision Therapy of Children and Adolescent Young Adults with Relapsed and Refractory Cancer: A Report from the Center for Cancer Research. Clin. Cancer Res. *22*, 3810–3820.

58. Gryder, B.E., Pomella, S., Sayers, C., Wu, X.S., Song, Y., Chiarella, A.M., Bagchi, S., Chou, H.C., Sinniah, R.S., Walton, A., et al. (2019). Histone hyperacetylation disrupts core gene regulatory architecture in rhabdomyosarcoma. Nat. Genet. *51*, 1714–1722.

59. Robinson, J.T., Thorvaldsdóttir, H., Winckler, W., Guttman, M., Lander, E.S., Getz, G., and Mesirov, J.P. (2011). Integrative genomics viewer. Nat. Biotechnol. *29*, 24–26.

60. Kuroda, H., Kutner, R.H., Bazan, N.G., and Reiser, J. (2009). Simplified lentivirus vector production in protein-free media using polyethylenimine-mediated transfection. J. Virol. Methods *157*, 113–121.

61. Tian, M., Cheuk, A.T., Wei, J.S., Abdelmaksoud, A., Chou, H.C., Milewski, D., Kelly, M.C., Song, Y.K., Dower, C.M., Li, N., et al. (2022). An optimized bicistronic chimeric antigen receptor against GPC2 or CD276 overcomes heterogeneous expression in neuroblastoma. J. Clin. Invest. *132*, e155621.

STAR★METHODS

KEY RESOURCES TABLE

REAGENT or RESOURCE	SOURCE	IDENTIFIER
Antibodies		
FGFR4 (D3B12) XP® Rabbit mAb	Cell Signaling Technology	Cat# CST8562; RRID:AB_10891199
Phycoerythrin (PE) conjugated mouse anti-human FGFR4 antibody (Clone 4FR6D3)	BioLegend	Cat# 324306; RRID:AB_2231698
Ultra-LEAF™ Purified Mouse IgG1, κ Isotype Ctrl Antibody	BioLegend	Cat# 401414
Ultra-LEAF™ Purified Human IgG1 Isotype Control Recombinant Antibody	BioLegend	Cat# 403502
3A11 mouse IgG antibody	This paper	N/A
3A11 scFvFc	This paper	N/A
Recombinant Anti-CD4 antibody [EPR6855]	Abcam	Cat# ab133616; RRID:AB_2750883
Recombinant Anti-CD8 alpha antibody [SP16]	Abcam	Cat# ab101500; RRID:AB_10710024
HRP-conjugated β-actin (C4)	Santa Cruz	Cat# sc-47778; RRID:AB_626632
Anti-rabbit, HRP labeled secondary antibody	Cell Signaling Technology	Cat# 7074S
FITC anti-human CD45 antibody	BioLegend, clone HI30	Cat# 304006; RRID:AB_314394
PE anti-human EGFR antibody	BioLegend, clone AY13	Cat# 352904; RRID:AB_10896794
PE anti-human CD3 antibody	BioLegend, clone HIT3a	Cat# 300308; RRID:AB_314044
PE-Dazzle594 anti-human CD4 antibody	BioLegend, clone A161A1	Cat# 357412; RRID:AB_2565664
APC anti-human CD8a antibody	BioLegend, clone RPA-T8	Cat# 301049; RRID:AB_2562054
Ghost Dye™ Violet 510	Cytek BioScience	SKU 13-0870-T100
Bacterial and virus strains		
NEB® Stable Competent E. coli (High Efficiency)	New England Biolabs	C3040H
Biological samples		
Human Alveolar rhabdomyosarcoma tissue microarrays (ARMS TMAs)	Children's Oncology Group (COG)	3000–30-P8967
Human embryonal rhabdomyosarcoma tissue microarrays (ERMS TMAs)	Children's Oncology Group	3000–30-P8968
COG Normal Pediatric TMA	Children's Oncology Group	N/A
human normal tissue microarray	US Biomax, Inc.	FDA999
Buffy Coats	NIH blood bank	N/A
human peripheral blood mononuclear cells (PBMCs)	NIH blood bank	N/A
Chemicals, peptides, and recombinant proteins		
Recombinant human FGFR1	Sino Biological	10616-H08H
Recombinant human FGFR2	Sino Biological	10824-H08H
Recombinant human FGFR3	Sino Biological	16486-H08H
Recombinant human FGFR4	Sino Biological	10538-H08H
Recombinant mouse FGFR4	Sino Biological	50194-M08H
Human IL-2	NIH pharmacy	N/A
D-Luciferin	PerkinElmer, Inc.	122799
Critical commercial assays		
V-PLEX human cytokine assay	Meso Scale Discovery (MSD)	Cat. K151AOH-2
Dynabeads Human T-Expander CD3/CD28	Thermo Fischer Scientific, Gibco	11141D
Lipofectamine 3000 Transfection Reagent	Thermo Fischer Scientific	L3000075
BD QuantiBRITE PE Beads	BD Biosciences	340495

(*Continued on next page*)

Continued

REAGENT or RESOURCE	SOURCE	IDENTIFIER
Deposited data		
dbGAP phs001928 for pediatric cancers	Brohl et al.[32]	https://www.ncbi.nlm.nih.gov/gap/
dbGaP phs000720 for RMS	Shern et al.[2]	https://www.ncbi.nlm.nih.gov/gap/
dbGaP phs001052 for Omics study	Chang et al.[57]	https://www.ncbi.nlm.nih.gov/gap/
TCGA data	https://portal.gdc.cancer.gov/	TCGA
Chromatin immunoprecipitation (ChIP) sequencing	Gryder et al.[58]	GSE116344
Experimental models: Cell lines		
RH30	Gryder et al.[58]	N/A
RH5	Gryder et al.[58]	N/A
RH41	Gryder et al.[58]	N/A
RH4	Gryder et al.[58]	N/A
JR	Gryder et al.[58]	N/A
RMS559	Dr. Jonathan Fletcher at Brigham and Women's Hospital, Boston, USA	N/A
BIRCH	Brohl et al.[32]	N/A
CTR	Brohl et al.[32]	N/A
RD	Brohl et al.[32]	N/A
RH30 FGFR4-KO	Dr. Michele Bernasconi at University Children's Hospital Zurich, Switzerland	N/A
RH4 FGFR4-KO	Dr. Michele Bernasconi at University Children's Hospital Zurich, Switzerland	N/A
7250	Gryder et al.[6]	N/A
RMS238	Gryder et al.[58]	N/A
RMS209	Gryder et al.[58]	N/A
RMS224	Gryder et al.[58]	N/A
SCMC	Gryder et al.[58]	N/A
NCI0082	Gryder et al.[58]	N/A
RH3	Gryder et al.[58]	N/A
RMS216	Gryder et al.[58]	N/A
SMS-CTR	Gryder et al.[58]	N/A
RMS206	Gryder et al.[58]	N/A
NCI0075	Gryder et al.[58]	N/A
RMS008	Gryder et al.[58]	N/A
JR1	Gryder et al.[58]	N/A
RH18	Gryder et al.[58]	N/A
Myoblasts	Gryder et al.[58]	N/A
Myotubes	Gryder et al.[58]	N/A
Psoas Muscle	Gryder et al.[58]	N/A
Skel. Muscle129	Gryder et al.[58]	N/A
Skel. Muscle134	Gryder et al.[58]	N/A
Human cardiomyocytes	Cellprogen	Cat# 36044-15
cholangiocytes	Cellprogen	Cat# 36755-12
pancreatic epithelial primary cells	Cellprogen	Cat# 36099-25
human coronary artery smooth muscle cells (CASMC)	Lonza	Cat# CC-2583
small airway epithelial cells (SAEC)	Lonza	Cat# CC-2547
bronchial/tracheal epithelial cells (NHBE)	Lonza	Cat# CC-2541
human renal epithelial cells (HRE)	Lonza	Cat# CC-2556
renal cortical epithelial cells (HREC)	Lonza	Cat# CC-2554
renal proximal tubule epithelial cells (RPTEC)	Lonza	Cat# CC-2553
hepatocytes	Lonza	Cat# HUCPG

(*Continued on next page*)

Continued

REAGENT or RESOURCE	SOURCE	IDENTIFIER
10 Donors pooled hepatocytes	Lonza	Cat# HUCS10P
HEK 293	ATCC	Cat# CRL-1573
Lenti-X 293T lentiviral packaging cell line	Clontech	632180
Experimental models: Organisms/strains		
NOD-scid IL2rgnull (NSG) mice	NCI CCR Animal Resource Program/NCI Biological Testing Branch	N/A
Recombinant DNA		
3A11-CD8HTM-BBz CAR	This paper	N/A
pMDLg/pRRE	Addgene	Plasmid #12251
PMD2.G	Addgene	Plasmid #12259
pRSV-Rev	Addgene	Plasmid #12253
Software and algorithms		
FlowJo v10.7.2	FlowJo, LLC	N/A
GraphPad Prism 8	GraphPad Software Inc.	N/A
Integrative Genomics Viewer (IGV)	Robinson et al.[59]	N/A
SnapGene 5.2.4	SnapGene	N/A
Image Lab	Bio-Rad	N/A
Aperio ImageScope	Leica Biosystem	N/A
RTCA software 2.0	Aligent	N/A
Living Image version (IVIS imaging)	Perkin Elmer	N/A
Biorender	Biorender	N/A
Other		
Zombie UV^{TM} Fixable Viability Kit	BioLegend	423108
CountBright Absolute Counting beads	Thermo Fischer Scientific	C36950

RESOURCE AVAILABILITY

Lead contact

Requests for further information and reagents should be directed to and will be fulfilled by the lead contact, Javed Khan (khanjav@mail.nih.gov).

Materials availability

Materials created in this study will be available for the scientific community by contacting the corresponding author and completion of a material transfer agreement.

Data and code availability

- The FGFR4 expression data for this study are available in dbGaP: phs000720, phs001928, phs001052, and https://portal.gdc.cancer.gov/for the TCGA data. ChIPSeq data have been deposited at Gene Expression Omnibus (GSE116344) and is publicly available.
- This paper does not report any original code.
- Any additional information required to reanalyze the data reported in this work paper is available from the lead contact upon request.

EXPERIMENTAL MODEL AND STUDY PARTICIPANT DETAILS

Cell lines

FGFR4 knock out cell lines (RH4 FGFR4-KO, RH30 FGFR4-KO) were gifts from Dr. Michele Bernasconi at University Children's Hospital Zurich, Switzerland. RMS559 was a gift from Dr. Jonathan Fletcher at Brigham and Women's Hospital, Boston, USA. HR, RD, CTR, RH5, 7250, RH4, RH4 FGFR4-KO, RH30, RH30 FGFR4-KO and RMS559 were all grown in Dulbecco Modified Eagle Medium (DMEM, Quality Biological) with 10% FBS (Life Technologies), 1% L-glutamine, and 1% penicillin–streptomycin. JR was cultured with RPMI 1640 supplemented with 10% FBS, 1% L-glutamine, and 1% penicillin–streptomycin at 37°C in a humidified atmosphere with

5% CO_2. All cell lines used were confirmed to be mycoplasma free by the MycoAlert kit (Lonza). STR DNA fingerprinting was performed for all cell lines used and confirmed their identity.

Primary cell culture

Peripheral blood mononuclear cells (PBMCs) obtained from blood of healthy donors were approved by NIH and isolated using Histopaque-1.077gm/mL (Sigma, Cat# 10771) according to the manufacturer's instructions.

Human cardiomyocytes (Cat# 36044-15), cholangiocytes (Cat# 36755-12), and pancreatic epithelial primary cells (Cat# 36099-25) were obtained from Cellprogen; human coronary artery smooth muscle cells (CASMC, Cat# CC-2583), small airway epithelial cells (SAEC, Cat# CC-2547), bronchial/tracheal epithelial cells (NHBE, Cat# CC-2541), human renal epithelial cells (HRE, Cat# CC-2556), renal cortical epithelial cells (HREC, Cat# CC-2554), renal proximal tubule epithelial cells (RPTEC, Cat# CC-2553), hepatocytes (Cat# HUCPG), and 10 Donors pooled hepatocytes (Cat# HUCS10P) were purchased from Lonza; HEK 293 cells (Cat# CRL-1573) was purchased from ATCC. All these cells were grown in special growth medium stated in their product information.

In vivo studies

Animal studies were conducted using 5∼8-week-old female NSG (NOD.Cg-Prkdcscid Il2rgtm1Wjl/SzJ) mice, obtained from NCI CCR Animal Resource Program/NCI Biological Testing Branch. They were housed and treated under the protocol (GB-011) approved by the NCI Bethesda Animal Care and Use Committee at the NIH.

Briefly, luciferase transduced RH30 or RMS559 cells were trypsinized and neutralized when they reached 80% confluency in a T175 flask. Cells were then washed two times with cold HBSS and injected into NSG mice. For intravenous (i.v.) injection, each mouse received 1E6 RMS cells in 0.2mL HBSS; for subcutaneous (s.c.) injection, each mouse received 1E6 RMS cells in 0.2mL HBSS containing 50% Matrigel (Corning). Three days later each mouse received i.v. 3E6 CAR T-cells, untransduced control (mock T), or HBSS vehicle control. For intramuscular (IM) injection, each mouse received 1E6 RH30 cells or 4E6 RH4 cells expressing luciferase, 10E6 CAR T-cells or mock T-cells were infused at day 7 post tumor implantation. Tumor engraftment was measured by a caliper or Xenogen IVIS Lumina imager (PerkinElmer). For Xenogen imaging, the mice were first injected with luciferin at 300 mg/kg and imaged 20 min later. Images were analyzed using Living Image, version 3.1 software (PerkinElmer) and the bioluminescent signal flux for each mouse was expressed as average radiance (photons/second/cm^2/steradian).

METHOD DETAILS

RNA-seq data analysis

RNA-seq data was analyzed as previously described.[32] Briefly, total RNAs was isolated from freshly frozen tumors and polyA-selected or Ribozero-selected RNA libraries were prepared for RNA sequencing on Illumina HiSeq2000, 2500, and NextSeq500 according to the manufactures protocol (Illumina, San Diego, CA). FastQC were used to assess for quality of paired end reads. And then fastq files were mapped to GRCH37 reference genome using the STAR/2.5.3a alignment algorithm and subsequently quantified by RSEM program based upon Ensembl GRCh37.75 gene annotation.

Chip-seq data analysis

Previously published ChIP-seq data of active histone mark H3K27ac was analyzed in RMS tumors and cell lines, both FP and FN-RMS, and compared to H3K27ac data in myoblasts, myotubes and muscle.[58] All samples were mapped to human genome build hg19 using BWA, and indexed BAMs were converted to compressed TDF format at 25 bp bin resolution after extension of reads to the median fragment length (∼200 bp extended past each mapped single-end, 75 bp read), using IGV command line tool toTDF. Files were visualized in IGV (https://software.broadinstitute.org/software/igv/download).

CRISPR data across the panel of cell lines was downloaded from Project Achilles (https://depmap.org/portal/).

Immunohistochemistry of normal tissue microarray (TMA) and RMS TMA

Normal tissue microarray (TMA) slide was purchased from US Biomax (FDA999w). Pediatric normal tissue TMA, aRMS TMA (P8967) and eRMS TMA (P8968) were obtained from the Children's Oncology Group. The TMA slides were deparaffinized with xylene and then dehydrated through a graded ethanol series. Antigen retrieval was performed for 20 min in heat-activated antigen retrieval buffer pH 6.0 (Dako, Carpinteria, CA) using a pressure cooker (Dako) followed by 10 min of blocking using 3% hydrogen peroxidase. The sections were incubated with rabbit monoclonal anti-FGFR4 antibodies (Clone D3B12; Cell Signaling; Denver, CA) at 1:150 for 1 h. Subsequently, the reaction of antigen-antibody reaction was detected by EnVision$^+$ Dual Link System-HRP (Dako) and visualized with DAB$^+$ (3, 3′-Diaminobenzidine; Dako). TMA sections were lightly counterstained in a Mayer's hematoxylin bath and then examined by light microscopy. Negative control rabbit immunoglobulin G (IgG) was used in place of a primary antibody to evaluate nonspecific staining and the TMA included appropriate positive control specimens. The stained sections were scanned using the NanoZoomer 2.0 HT (Hamamatsu Photonics K.K., Japan) at 20× objective magnification. Immunohistochemistry staining results were reviewed by a board-certified pathologist and H score was determined based on the staining intensity and percentage of

positive stained cells using the formula: H-score = [(0 × % negative cells) + (1 × %weakly positive cells) + (2 × %moderately positive cells) + (3 × %strongly positive cells)]. For multiple cores with the same type of sample from the sample individual, only the highest H score was used for data analysis.

Generation of 3A11 scFvFc

3A11 is a mouse IgG that was developed from mice immunized with human FGFR4 Fc (R&D). The variable heavy and light chains encoding the scFv, were cloned into a plasmid containing the constant fragment (Fc) of human IgG1, thus creating the scFvFc expression vector. This scFvFc plasmid was transiently expressed in Expi293 system (Life Technologies). Protein was then purified by Affinity chromatography (GE Biosciences). The purified scFvFc fusion protein was analyzed by nanodrop for size and impurities.

ELISA assay

Recombinant human FGFR1-4 (Sino Sino Biological) proteins were coated on Corning EIA/RIA high binding 96 well plate (Corning, Inc) at 50ng per well for overnight at 4°C and blocked with 3% BSA in PBS. 3A11 scFvFc, at a starting concentration of 1000 ng/μL was further serially diluted to 3 ng/μL, added, and incubated at room temperature for 2 h. The plates were washed with PBS containing 0.05% Tween 20. Bound 3A11 scFvFc was detected by a goat anti-human IgG (Fc specific)- peroxidase (Jackson Laboratory). The assay was developed at room temperature with ABTS substrate (Roche) and absorbance quantified at 405nm.

3A11 scFvFc binding affinity determined by octet analysis system

The binding kinetics of the 3A11 scFvFc was determined by the Octet RED96 system (FortéBio) using Bio-Layer Interferometry (BLI). 3A11scFvFc protein was resuspended in 0.1% BSA, 0.1% Tween 20 PBS, pH 7.4 buffer. FGFR4 ECD protein was immobilized onto biosensors, 3A11 scFvFc was injected and allowed to flow through the sensor. The relative association measurements for a time window of 600 s and 1,400 s, respectively was collected. Data analysis was performed using the analysis software provided with the instrument. The KD value of 3A11 scFvFc was determined by global fitting analysis and 2:1 binding model.

Electrochemiluminescence assay

Normal human tissues were cut in small size, and lysates were prepared using Fastprep 24 homogenizer and lyser. RMS cell lysates were prepared using cell lysis buffer, RIPA and protease inhibitors. Both the tissue and cell lysates, after lysis, were processed by incubation on ice for 30 min in the lysis buffer. The lysates were centrifuged at 13200rpm for 10 min at 4C. The supernatant was isolated and used to measure total protein using BCA assay. All lysates were further diluted to a final total protein concentration of 1 mg/mL 25μL of this concentrate was used in Duoset ELISA kit that measures total human FGFR4. The detection reagent was conjugated as described by MSD Gold Sulfo Tag NHS-Ester kit. Recombinant FGFR4 protein, also supplied by the ELISA kit, was used to generate a standard curve, to quantify the amount of FGFR4 in tissue and cell lysates.

Western blot analysis

Western blot analysis was performed as previously described. Briefly whole cell lysates were prepared using RIPA buffer supplemented with protease and phosphatase inhibitors. Cells were lysed by sonication, rotated for 30 min at 4°C, and then lysates were centrifuged for 10 min, supernatant removed, and protein concentration quantified using a Bradford assay. 20 μg of lysate protein was resolved on 4–12% Bis-Tris gels and transferred to PVDF membrane, blocked in 5% nonfat milk in Tris-buffered saline and Tween 20 (TBS-T). Membranes were incubated at 4°C overnight in primary antibody, washed x 3 in TBS-T, then incubated in 1:2,000 diluted anti-rabbit, HRP-labeled secondary antibody (Cell Signaling Technology, Cat# 7074S) at room temperature for 1 h, washed an additional × 3 with TBST, and then developed with chemiluminescent reagents. The following antibodies were used: HRP-conjugated β-actin (Santa Cruz, C4, sc-47778); FGFR4 XP Rabbit mAb (Cell Signaling Technology, clone D3B12, CST8562).

Cell surface protein determination assay

1E6 RMS cell were detached from culturing flasks by 0.05% trypsin and then washed twice with cold PBS and resuspended in 100μL of cold FACS buffer (1× PBS, 22% FBS, 2mM EDTA and 25mM HEPES). Cells were incubated with 5μg of anti-FGFR4 mAb (Clone 4FR6D3, mouse anti-FGFR4 PE, BioLegend, Cat # 324306) or 1μg of 3A11 scFvFc or their isotype control, for 30 min at 4°C. After incubation, cells were washed twice with FACS buffer and resuspended in secondary goat anti mouse or human antibody (Jackson Laboratory) at 1:200 dilution in FACS buffer. Following incubation, cells were washed three times with FACS buffer. Stained cells were analyzed on BD FACS Caliber or LSRFortessa. Data was analyzed and MFI was calculated for FGFR4 surface levels measurement by using Flow Jo software. FGFR4 surface molecules per cell were calculated post subtracting background signal emanating from a respective isotype control antibody (Clone QA16A12 for human IgG1 antibody, Biolegend) by the Quantibrite PE Quantitation Kit (BD Biosciences, Cat# 340495) according to the manufacturer's protocol.

Generation of the 3A11 CAR construct and lentivirus production

The FGFR4 CAR contains the targeting scFv sequence derived from a mouse 3A11 monoclonal antibody. The scFv sequence was linked in frame to CD8 hinge and transmembrane domain, 4-1BB/CD137 co-stimulatory domain, and CD3ζ activation domain. Leader sequence from CD8 alpha subunit was included upstream of the CAR, to facilitate CAR expression at the cell surface

membrane. CAR sequence was followed by the ribosomal skip element T2A and the truncated epidermal growth factor receptor sequence (tEGFR, NP_958441.1, AA 334–627), used as a safety tag. The CAR expression cassette was cloned into a third-generation lentiviral plasmid backbone (Lentigen Technology, Gaithersburg, MD) under the regulation of a human EF-1α promoter. Clinical grade lentiviral vector (LV)-containing supernatants were generated by transient transfection of HEK 293 T-cells[60] was used for all experiments except for efficacy testing in the RH4 IM model in Figure 7, which used in-house manufactured process as described previously.[61] Harvested lentivirus supernatants were stored at −80°C.

3A11 CAR T cell manufacturing

Clinical grade 3A11 CAR T-cells were manufactured on the automated closed-system CliniMACS Prodigy (Miltenyi Biotec). Cultures were initiated from thawed CD4/CD8 T-cells that were previously selected on the CliniMACS Prodigy from healthy donor apheresis products. On Day 0 of culture, approximately 100E6 thawed CD4/CD8 T-cells were initiated on the Prodigy in TexMACS media (Miltenyi Biotec) supplemented with 3% human AB serum (Valley Biomedical) and 200 IU/mL IL-2 (Clinigen Inc.) and stimulated with TransAct anti-CD3/CD28 polymeric nanomatrix (Miltenyi Biotec). On Day 1, cells were transduced with FGFR4 lentiviral vector at a multiplicity of infection (MOI) of 20. On Day 3, transduction was stopped and TransAct was washed out, and a series of media addition/exchanges were performed daily on Days 5–8. On Day 9, the final product was collected and cryopreserved. For efficacy testing in the RH4 IM model in Figure 7, we used in-house CAR T cell production as described previously.[61]

xCELLigence Real-Time Cell Analysis and cytokine release assay

5000 target cells were seeded in each well of 96 E-plate (Roche). Cells were monitored continuously by the xCELLigence system. Six hours later, CAR T-cells and its mock T (un-transduced) controls at different E:T ratio and cells were added and continuously monitored for further 18 h. At the endpoint, cells were spun down, and supernatant was collected. V-PLEX Custom Human Biomarkers Proinflammatory Panel1 (Human IFN-γ, Human IL-2 and Human TNF-α, Meso Scale Discovery) was used to measure the cytokine level in the supernatant as per manufactory's instruction.

In vitro toxicity study

For each of the toxicity experiment, 7250 and human RMS cells RH30 was used as negative and positive controls respectively. Briefly, controls and cells to be tested were first seeded in each well of 96 well flat bottom plate for 6 h. Then all culture medium for controls was replaced with culture medium used for the primary cells (DMEM for HEK293), CAR T-cells in the primary cell culture medium was then added at an E:T ratio of 1:1. Eighteen hours later, all cells were spun down and supernatant were taken for cytokine release assay. Since the growth medium is optimized for the primary cells and therefore may not be optimized for CAR T-cells, for each culture condition, the cytokine released was normalized with the cytokine detected in the positive control by the following formula: log2 (primary/RH30).

CAR T-cells persistence and exhaustion analysis by flow cytometry

For CAR T cell persistence analysis, splenocytes were isolated from RMS559 i.v. xenografted mice at day 70 post CAR T cell infusion. Blood was collected from RH30 IM xenografted mice at day 35 or RH4 IM implanted mice at day 42 post CAR T-cells treatment and then red blood cell (RBC) was lysed by RBC Lysis Buffer (BioLegend, 10×, Cat# 420301) before flow cytometry antibodies staining. T-cells were detected using the following anti-human antibodies: CD45-FITC (BioLegend, clone HI30), CD3-PE (BioLegend, clone HIT3a), CD4-PE-Dazzle594 (BioLegend, clone A161A1), CD8-APC (BioLegend, clone RPA-T8), EGFR-PE (BioLegend, clone AY13). The absolute CAR T cell counts in the spleen from tumor-bearing NSG mice were measured by using CountBright absolute counting beads for flow cytometry (Invitrogen) according to the manufacturer's protocol. All staining was performed in 0.1 mL FACS buffer (PBS +0.5% BSA + 2mM EDTA). Flow cytometry was performed using a FACS LSRFortessa (BD Biosciences) and data analyzed with FlowJo software (Tree Star).

H&E and immunohistochemistry (IHC) for tumor infiltrating T-cells

Formalin-fixed tumors from RH30 subcutaneous xenograft model were embedded in paraffin, and 5 μm FFPE thick sections were cut and mounted for staining. Sections of neoplastic masses occasionally contained adjacent normal tissues, including fibroadipose connective tissue and skeletal muscle.

IHC was performed using CD4 (1:250 dilution, Abcam, Cat# Ab133616), CD8 (1:100 dilution, Abcam, Cat# Ab101500), FGFR4 (1:100 dilution, Cell Signaling Technology, Cat# CST8562). Positive IHC controls included human tonsil and cell pellets known to be positive and negative for FGFR4. Negative controls included replacing the primary antibody with nonspecific antibody from the same species and of the same isotype.

Whole Slide Imaging (WSI) was performed with an Aperio ScanScope XT (Leica) at 200× in a single z-plane. Annotations were made to include tumor tissue and exclude tumor necrosis and section artifacts for IHC quantification. Digital pathology for biomarker quantification was performed following WSI. Thresholds for positivity was determined using known positive controls. Tumor necrosis was estimated by a pathologist as % area from H&E images. CD4 and CD8 positive cells are reported as number of positive cells per mm^2.

QUANTIFICATION AND STATISTICAL ANALYSIS

Statistical analysis

GraphPad Prism software was used for data analysis. Log rank statistics was used for calculation of p value of survival analyses, two-way repeated measures (RM) ANOVA or mixed-effect analysis was used for calculating significant difference of tumor growth curves, and two-way ANOVA was used for p value calculation of *in vitro* cytokines production data. $p < 0.05$ was considered statistically significant, and p values are denoted with asterisks as follows: $p > 0.05$; not significant, ns; *$p < 0.05$; **$p < 0.01$; ***$p < 0.001$; and ****$p < 0.0001$.

Cell Reports Medicine, Volume *4*

Supplemental information

Preclinical development of a chimeric antigen receptor T cell therapy targeting FGFR4 in rhabdomyosarcoma

Meijie Tian, Jun S. Wei, Nityashree Shivaprasad, Steven L. Highfill, Berkley E. Gryder, David Milewski, G. Tom Brown, Larry Moses, Hannah Song, Jerry T. Wu, Peter Azorsa, Jeetendra Kumar, Dina Schneider, Hsien-Chao Chou, Young K. Song, Abdelrahman Rahmy, Katherine E. Masih, Yong Yean Kim, Brian Belyea, Corinne M. Linardic, Boro Dropulic, Peter M. Sullivan, Poul H. Sorensen, Dimiter S. Dimitrov, John M. Maris, Crystal L. Mackall, Rimas J. Orentas, Adam T. Cheuk, and Javed Khan

Supplementary information

Preclinical development of a Chimeric Antigen Receptor T-cell therapy targeting FGFR4 in rhabdomyosarcoma

Meijie Tian, Jun S. Wei, Nityashree Shivaprasad, Steven L. Highfill, Berkley E. Gryder, David Milewski, G Tom Brown, Larry Moses, Hannah Song, Jerry T. Wu, Peter Azorsa, Jeetendra Kumar, Dina Schneider, Hsien-Chao Chou, Young K. Song, Abdelrahman Rahmy, Katherine E. Masih, Yong Yean Kim, Brian Belyea, Corinne M. Linardic, Boro Dropulic, Peter M. Sullivan, Poul H. Sorensen, Dimiter S. Dimitrov, John M. Maris, Crystal L. Mackall, Rimas J. Orentas, Adam T. Cheuk, and Javed Khan

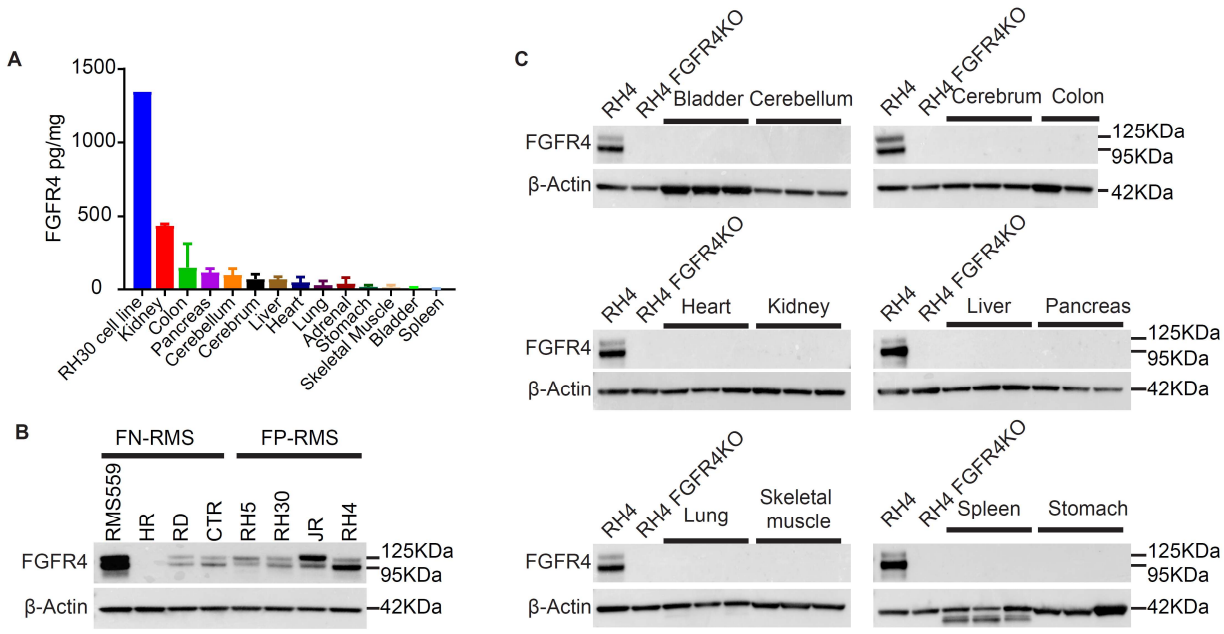

Figure S1. Protein expression of FGFR4 in RMS cell lines and normal organs. Related to Figure 1. (A) FGFR4 protein is expressed at lower levels in normal tissues by electrochemiluminescence assay compared to the positive control FP-RMS cell line RH30. **(B)** FGFR4 protein is expressed in FP-RMS and some FN-RMS cell lines by Western. **(C)** FGFR4 expression is only detected in RH30 but not in normal tissues.

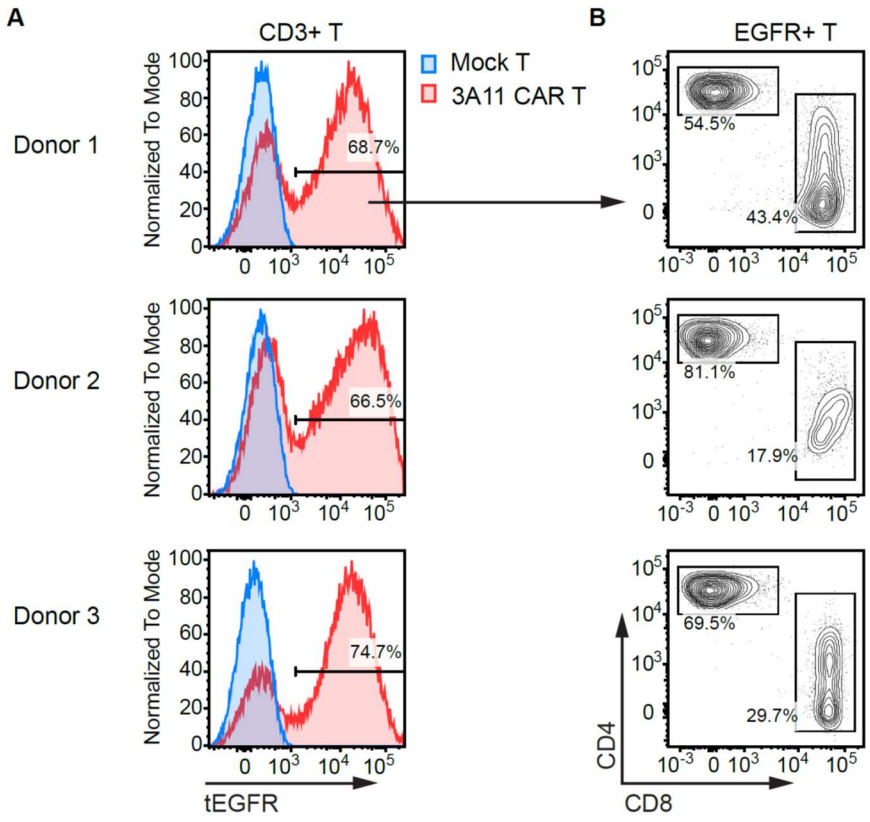

Figure S2. Transduction efficiency of 3A11 CAR T-cells manufactured using the CliniMACS® Prodigy system from three healthy donors. Related to Figure 4. (A) Representative flow cytometry plots show the transduction efficiency of 3A11 CAR T-cells by staining with EGFR antibody. **(B)** The percentages of $CD4^+$ or $CD8^+$ CAR T-cells gating on the $EGFR^+$ T-cells are shown.

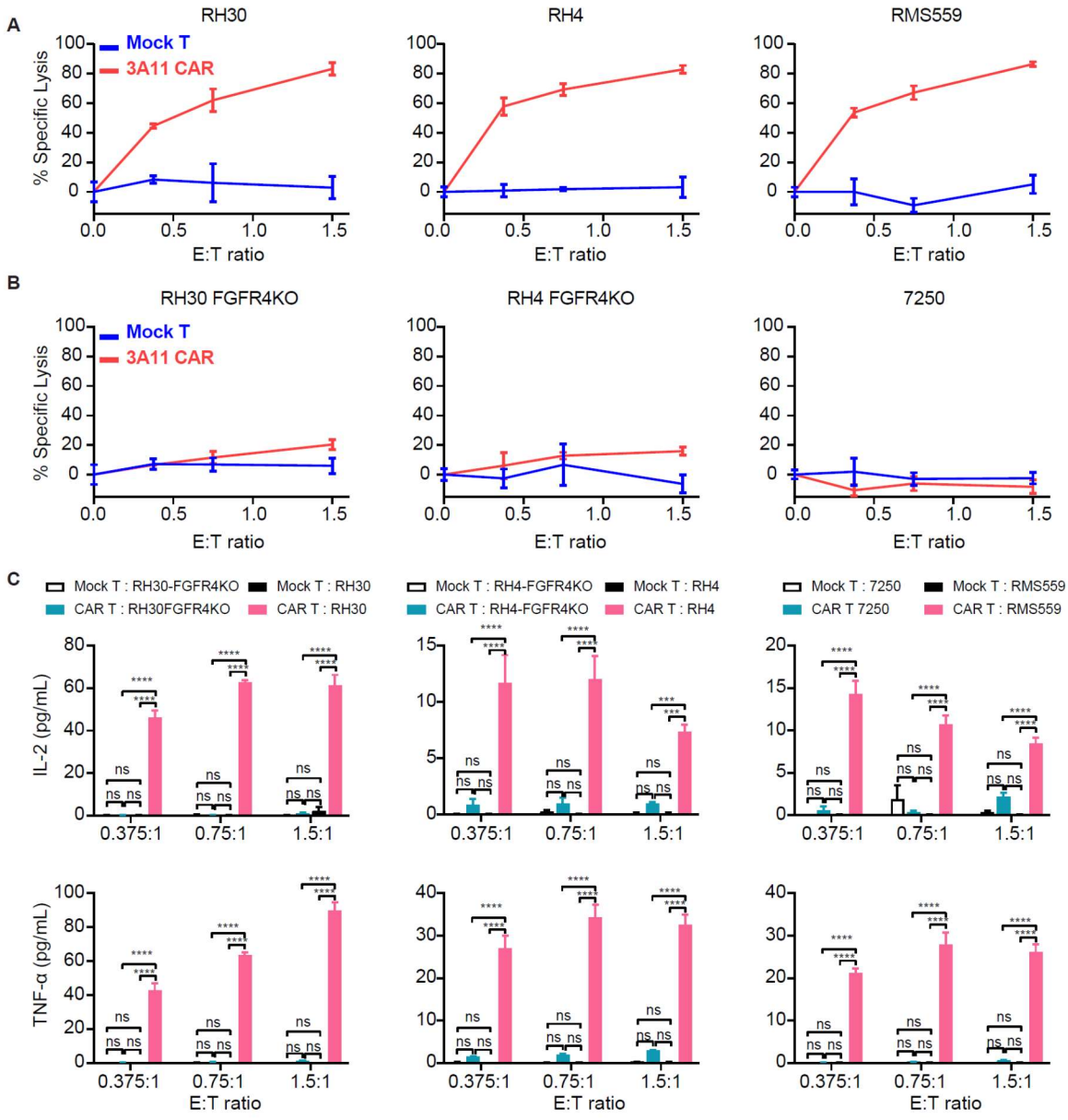

Figure S3. 3A11 CAR T-cells show specific killing activity to FGFR4 expressing RMS tumor cells. Related to Figure 4. (**A** and **B**) The specific lysis percentage of 3A11 CAR T-cells co-cultured with FGFR4 expressing RMS cells (**A**) or with RH30 FGFR4-KO, RH4 FGFR4-KO or human fibroblast cell line 7250 (**B**) at the indicated E:T ratios in an RTCA. (**C**) IL-2 and TNF-α production levels of 3A11 CAR T-cells following a 20-hour co-culture with FGFR4 expressing RMS cells or FGFR4-KO or 7250 are shown. Values represent mean ± SEM. Statistical test represents two-way ANOVA multiple comparisons (****$p < 0.0001$, ***$p < 0.01$, **$p < 0.01$, *$p < 0.05$; ns, $p > 0.05$).

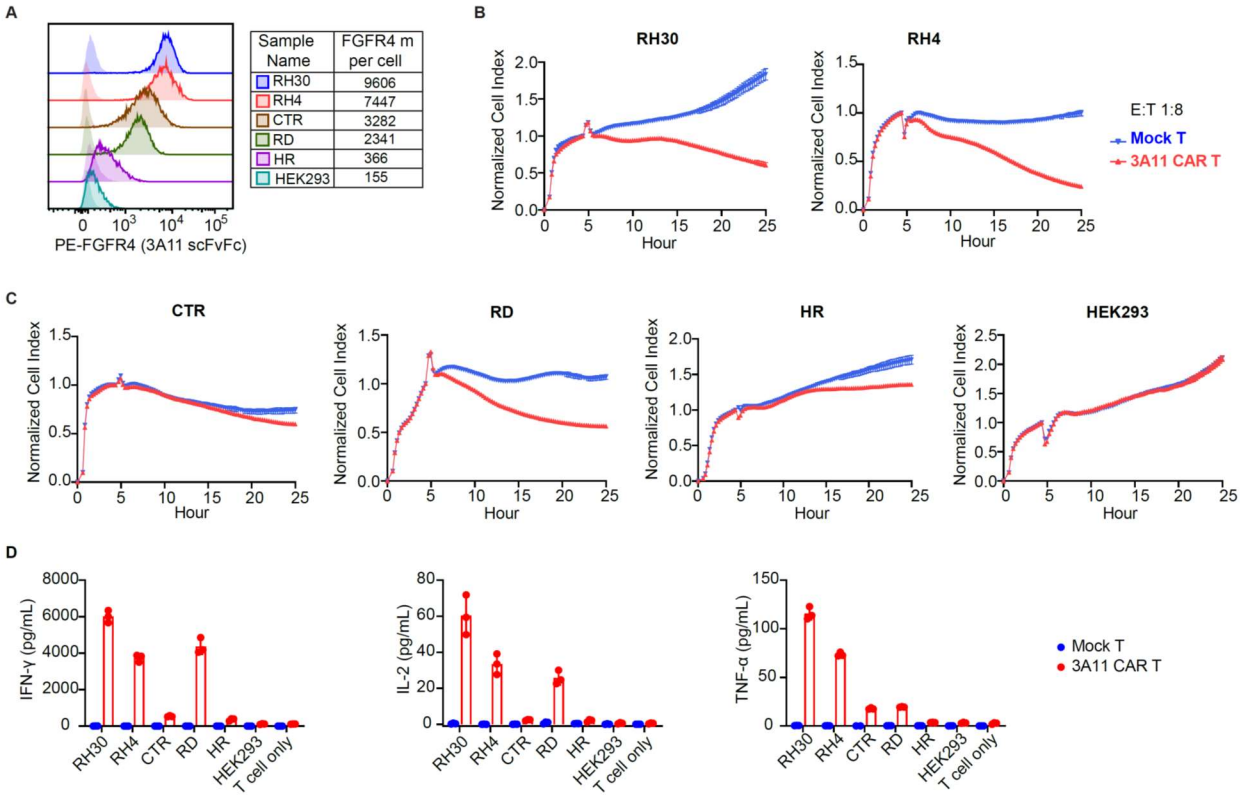

Figure S4. 3A11 CAR T-cells exhibited low/absent antitumor activity when co-culturing with cells expressing low levels of FGFR4, such as HR or HEK293 cells. Related to Figure 5. (A) Representative flow cytometry plot showing differential levels of FGFR4 expression on RMS cell lines and normal cell HEK293. And Surface FGFR4 molecule numbers/cell of indicated cell lines listed in the right table are estimated and quantified by PE quantitation beads. (B and C) Cytotoxicity assays show the differential killing activity of 3A11 CAR T-cells to different RMS cell lines or HEK293 with variable FGFR4 expression levels at an E:T ratio of 1:8. (D) Cytokine release assays show 3A11 CAR T-cells only release high-level cytokine when co-cultured with RH30, RH4, or RD cells, rather than the CTR, HR, or HEK293 cells. These data are consistent with their killing ability. Values in (B) and (C) represents mean ± SEM. Values in (D)represents mean ± SD. Representative of $n = 2$ independent experiments with $n = 2$ individual donors.

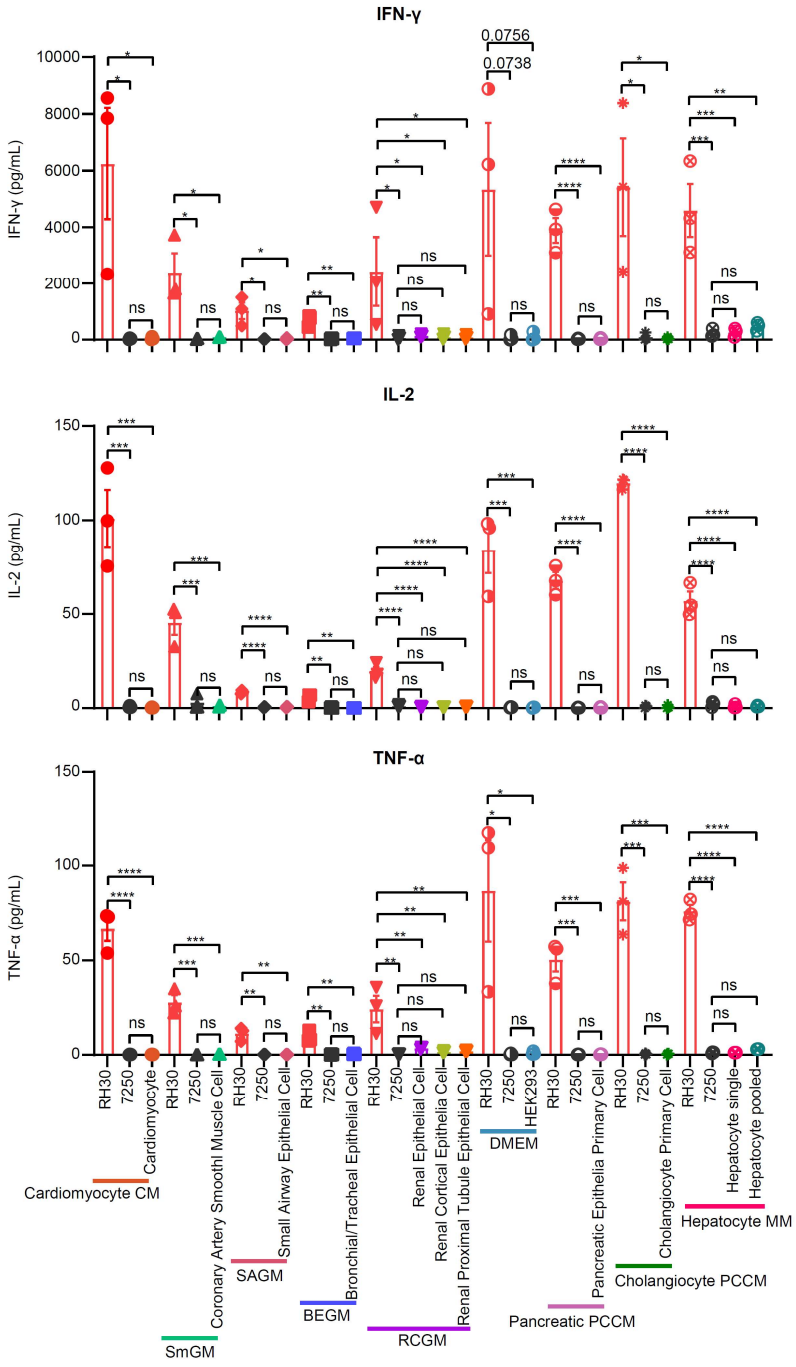

Figure S5. 3A11 CAR T-cells exhibited similar low cytokine production when co-culturing with primary cells as 7250 cells. Related to Figure 5. Cytokine (IFN-γ, IL-2, or TNF-α) released by FGFR4 CAR T-cells from three individual donors when coculturing with primary cells or the FGFR4 negative cell line 7250, compared to the positive cell RH30, grown in their respective media. Statistics represent ordinary one-way ANOVA (****$p < 0.0001$, ***$p < 0.01$, **$p < 0.01$, *$p < 0.05$; ns, $p > 0.05$). Values show $n = 3$ independent experiments with $n = 3$ individual donors.

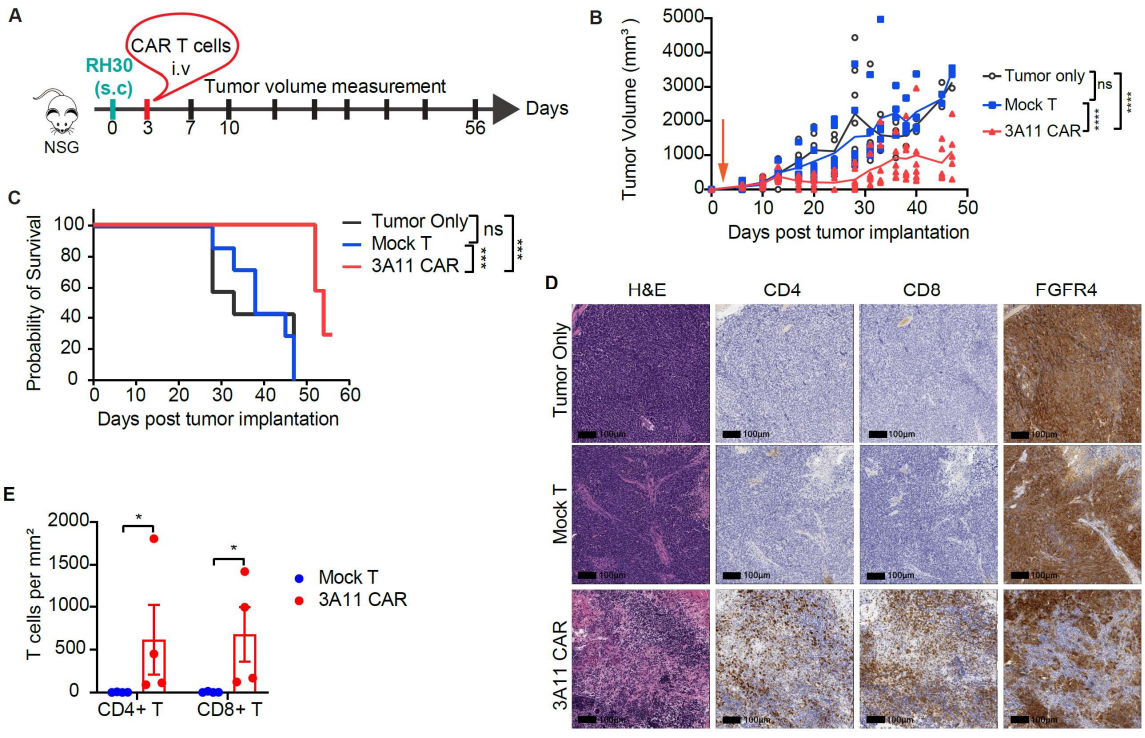

Figure S6. 3A11 CAR T-cells successfully infiltrate into a solid subcutaneous RMS tumor. Related to Figure 7. (**A**) Schema of the RH30 subcutaneous xenograft model infused with HBSS vehicle, mock or 3E6 CAR T-cells on day 3 post tumor inoculation. (**B**) Individual RH30 tumor volume after receiving mock or CAR T-cells treatment was measured by caliper. Arrow indicated the day that mice received treatment. Means and each replicate are shown, n = 7. Mixed-effects analysis is used to calculate the p values between each two groups individually. ****$p < 0.0001$. (**C**) Kaplan-Meier survival analysis of mice receiving different treatments are shown. Tumor only vs 3A11 CAR ***p = 0.0003; for mock T vs 3A11 CAR ***p = 0.0002. (**D**) Representative images of H&E, IHC staining within RH30 tumor grafts from mice treated with HBSS, mock T-cells and 3A11 CAR T-cells individually. All tumors are intensely positive for FGFR4. 3A11 CAR T-cells treated mice typically harbor small tumors that contain significant CD4 and CD8 positive tumor infiltrating lymphocytes. Rare CD4 and CD8 positive cells are observed in mock T-cell treated tumors. Scale bars labeled on image is 100µm, n = 4. (**E**) $CD4^+$ or $CD8^+$ T-cells significantly infiltrating into tumors treated with 3A11 CAR T-cells. Annotations were made to include tumor tissue and exclude tumor necrosis and section artifact for quantification of IHC. Digital pathology for biomarker quantification was performed following Whole Slide Imaging (WSI). Thresholds for positivity was determined using known positive controls. $CD4^+$ and $CD8^+$ T-cells are reported as number of positive cells per mm^2 of slide area. Mann-Whitney test was used to calculate the p value. * $p < 0.05$.

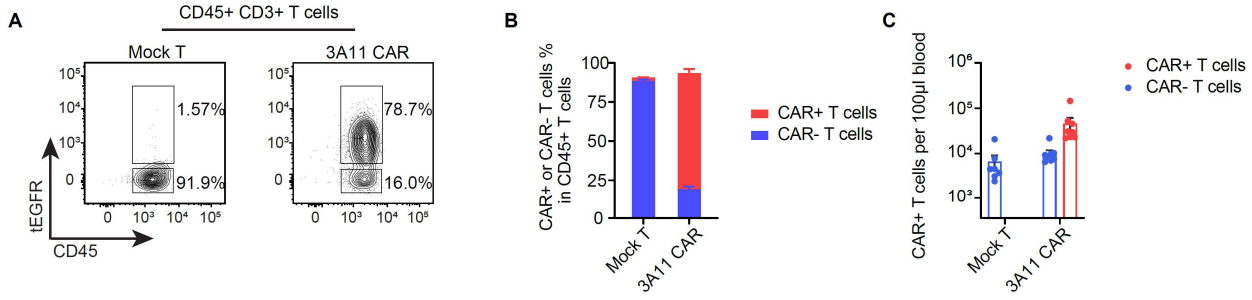

Figure S7. 3A11 CAR T-cells phenotype in RH4 orthotopic tumor model. Related to Figure 7. (A) Representative flow cytometric plots of CAR T-cell percentages in $CD45^+$ $CD3^+$ T-cells of blood collected from above mice at day 49 post RH4 implant. (B and C) Percentage of CAR^+ and CAR^- in $CD45^+$ $CD3^+$ T-cells from PBMCs (B) and total counts of the indicated T-cells in 100µl blood (C). Data are shown as the mean ± SEM (*n* = 7 or 8).